Received: 26 January 2021 | Revised: 7 March 2021 | Accepted: 12 March 2021

DOI: 10.1002/aoc.6246

FULL PAPER

Applied Organometallic Chemistry WILEY

Spectroscopic, density functional theory, nonlinear optical properties and in vitro biological studies of Co(II), Ni(II), and Cu(II) complexes of hydrazide Schiff base derivatives

Ramadan M. Ramadan[1] | **Samir M. El-Medani**[2] | **Abdelmoneim Makhlouf**[2] | **Hussein Moustafa**[3] | **Manal A. Afifi**[2] | **Matti Haukka**[4] | **Ayman Abdel Aziz**[1]

[1]Chemistry Department, Faculty of Science, Ain Shams University, Cairo, Egypt

[2]Department of Chemistry, Faculty of Science, Fayoum University, Fayoum, Egypt

[3]Department of Chemistry, Faculty of Science, Cairo University, Giza, Egypt

[4]Department of Chemistry, University of Jyvaskyla, PO Box 35, Jyvaskyla, Finland

Correspondence
Ramadan M. Ramadan, Chemistry Department, Faculty of Science, Ain Shams University, Cairo, Egypt.
Email: rmramadan@sci.asu.edu.eg

Complexes of three molecularly designed phenylacetohydrazide Schiff base derivatives—*N*′-(2-hydroxybenzylidene)-2-phenylacetohydrazid (**HL**^{1}), *N*-(1-(2-hydroxyphenyl)ethylidene)-2-phenylacetohydrazide (**HL**^{2}), and *N*′-((1-hydroxynaphthalen-2-yl)methylene)-2-phenylacetohydrazide (**HL**^{3})—with some bivalent metal ions were synthesized and investigated by several spectroscopic and analytical techniques. The crystal structure of **HL**^{1} ligand has been solved by conventional X-ray diffraction technique. Molecular geometries of **HL**^{1} and the studied complexes were investigated using the DFT-B3LYP/GENECP level of theory. Quantum and non-quantum global reactivity descriptors as well as the nonlinear optical properties were calculated. Biological parameters such as antimicrobial and antioxidant activities, fluorescence quenching studies, and viscosity measurements of the complexes were carried out. Molecular docking studies of **HL**^{1} and complexes using Molecular Operating Environment (MOE) software are reported. The different biological studies and the molecular docking were correlated to each other. The biological studies supported that the complexes can bind to DNA via intercalative mode and showed a various DNA binding potency.

KEYWORDS

biological activity, CT-DNA binding, DFT studies, molecular docking, nonlinear optical properties, X-ray analysis

1 | INTRODUCTION

In the last two decades, the necessity to prepare and develop novel antibacterial drugs with better mechanism of action and structure–activity relationship becomes vital biomedical need.[1] Schiff base ligands, especially those having hydrazide–hydrazone moiety [–(C=O)NHN=CH], were found to be excellent pharmacophores for designing and developing various biologically active materials.[2–4] These bases as well as their metal complexes are widely used in different applications such as anticancer, anti-HIV, antiradical, antibacterial, antifungal, and DNA cleavage.[5–7] In addition, hydrazide derivatives were found to possess a broad spectrum of antibacterial activities. Also, they can act as a good potential for oral drugs used, for example, in the treatment of genetic disorders like thalassemia.[8,9] Interest in binding of metal complexes to nucleic acids (DNA and RNA) was motivated to understand the basics of these interaction modes as well as the development of metal complexes to use them as

anti-inflammatory or anticancer drugs.[10] Several series of important hydrazide–hydrazone derivatives were found to have promising anticancer activities.[11–13] Also, some transition metal hydrazone complexes such as zinc(II) and nickel(II) complexes were found to have anti-inflammatory, antibacterial, anticancer, antihypertensive, and DNA-binding activities.[14,15] Furthermore, complexes of some transition metals such as cobalt(II), nickel(II), and copper(II) presented various biochemical actions either as essential trace metals or as a constituent of different exogenously administered compounds in humans. These complexes were also found to be serious in vitro and in vivo bioactive species. Importance of these derivatives appeared from their increasing interest as potential drugs for therapeutic intervention in various diseases.[16–19] Recently, we reported the synthesis and spectroscopic, structural, and theoretical studies along with the biological properties of two molecularly designed hydrazone ligands derived from phenylacetohydrazide as well as their Cu(II) complexes.[2] In order to continue our investigations of these Schiff base derivatives, here we report the synthesis and the X-ray analysis of another new hydrazone ligand, **HL^1** (Scheme 1). Also, the synthesis and spectroscopic and theoretical studies as well as the biological properties of cobalt(II), nickel(II), and copper(II) complexes of that ligand and its related ligands (**HL^2** and **HL^3**; Scheme 1) are reported.

2 | EXPERIMENTAL

2.1 | Reagents

The reported chemicals and reagents (analytical reagent grade) in this study were used without further purification. 2-Phenylacetohydrazide, salicylaldehyde (d = 1.146, 98%), and organic solvents were provided from Fluka. Co $(NO_3)_2{\cdot}6H_2O$, Ni $(CH_3COO)_2{\cdot}4H_2O$, and Cu $(CH_3COO)_2{\cdot}H_2O$ were provided from Sigma-Aldrich. All other chemicals used in this study were purchased from Fluka.

2.2 | Instrumentation

Infrared measurements were carried out using a Unicam Mattson 1000 FTIR spectrometer using KBr discs. Electronic absorption spectra were recorded on a Unicam UV2-300 UV–VIS spectrophotometer. Fluorescence measurements were done on a Jenway 6270 fluorimeter. The excitation source was a pulsed xenon lamp. Nuclear magnetic resonance (NMR) measurements were carried out on a Bruker BioSpin 300-MHz spectrometer using DMSO-d_6 solvent. Magnetic susceptibilities of the complexes (Gouy's method) were measured using a Sherwood Scientific magnetic balance. Elemental analyses were carried out using a PerkinElmer 2400 CHN elemental analyzer. Mass spectra of solid complexes (70 eV, EI) were performed on a Finnigan MAT SSQ 7000 spectrometer. Thermogravimetric (TG) analysis were done under stream of nitrogen gas (heating rate = 10°C/min) using a Shimadzu DT-50 thermal analyzer. Conductivity measurements were carried out in dimethyl sulfoxide (DMSO) (1×10^{-3} M, 25°C) using Jenway 4010 conductivity meter.

2.3 | Preparations of ligands

2.3.1 | Preparation of (E)-*N′*-(2-hydroxybenzylidene)-2-phenylacetohydrazid, HL^1

A mixture of 2-phenylacetohydrazide (0.01 mol, 1.5 g) and salicylaldehyde (0.01 mol, 1.06 g = 0.95 mL) was

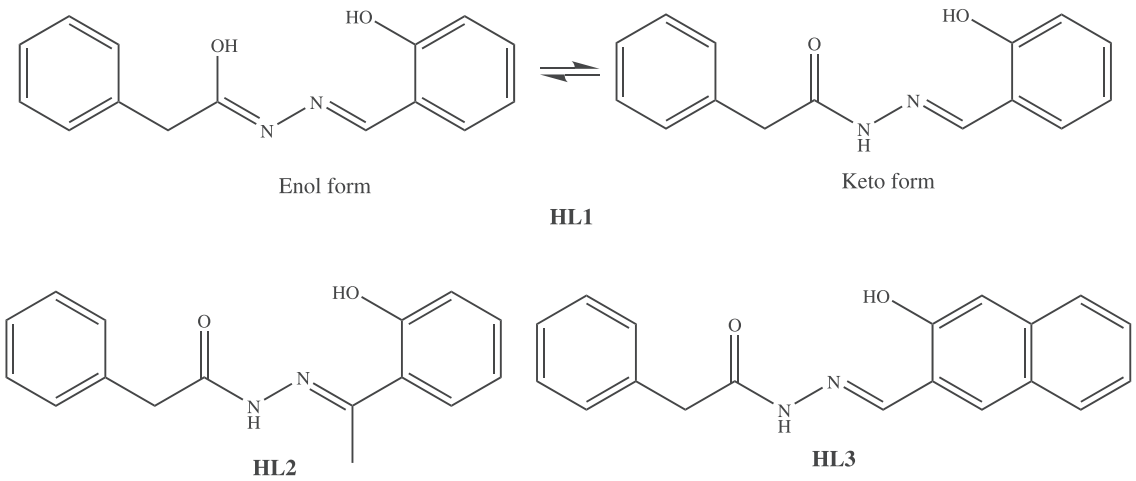

SCHEME 1 Structure of the ligands

refluxed in absolute ethanol for 3 h at which a brown product was separated. The residue was filtered off and then washed several times with cold ethanol. The product was recrystallized from hot ethanol to yield a crystalline brown product.

2.3.2 | Preparation of *N*-(1-(2-hydroxyphenyl)ethylidene)-2-phenylacetohydrazide, HL^2

The $\mathbf{HL^2}$ ligand was prepared as described before[2]: A mixture of 2-phenylacetohydrazide (0.01 mol, 1.5 g) and 2′-hydroxyacetophenone (0.01 mol, 1.2 mL) was refluxed in absolute ethanol for 3 h at which a yellow product was separated. The residue was filtered off, washed with cold ethanol for several times, and then recrystallized from hot ethanol to give a crystalline yellow product (yield = 80%).

2.3.3 | *Preparation of* N′-((1-hydroxynaphthalen-2-yl)methylene)-2-phenylacetohydrazide, HL^3

Similar procedure as that used for the preparation of $\mathbf{HL^2}$ was performed with the use of a mixture of 2-phenylacetohydrazide (0.01 mol, 1.5 g) and 1-hydroxy-2-naphthaldehyde (0.01 mol, 1.72 mL). Yellow crystalline product was separated after recrystallization from ethyl acetate (yield = 75%).

2.4 | Synthesis of complexes

2.4.1 | Synthesis $[Co(L^1)_2]$ complex

To an ethanolic solution of $\mathbf{HL^1}$ (1.9 mmol, 0.50 g) was added to an aqueous solution of Co $(NO_3)_2$ (1.9 mmol, 0.55 g) drop by drop. The mixture was refluxed for 3 h. The reaction mixture was left to stand at room temperature for few hours. The separated orange residue was filtered off and washed several times with cold ethanol and ether. The crude was then recrystallized from hot ethanol to give fine crystalline product.

2.4.2 | Synthesis $[Ni(L^1)_2]$ and $[Cu(L^1)_2]\cdot 2H_2O$ complexes

Similar procedure was employed as that used for the synthesis of $\mathbf{[Co(L^1)_2]}$ complex with the use of either Ni $(CH_3COO)_2$ (1.9 mmol, 0.47 g) or Cu $(CH_3COO)_2$ (1.9 mmol, 0.37 g). The crude complex was recrystallized from hot ethanol to give faint green crystals for nickel complex and green crystals for copper derivative.

2.4.3 | Synthesis $[Ni(L^2)_2]$, $[Co(L^3)_2]\cdot 2H_2O$, and $[(NiL^3)_2]$ complexes

Similar procedure as that used for the preparation of complexes of $\mathbf{HL^1}$ was performed with the use of the other two ligands ($\mathbf{HL^2}$ and $\mathbf{HL^3}$).

Color, yield, elemental analysis, and mass spectral and effective magnetic moment data for the reported derivatives are given in Table 1.

2.5 | X-ray structure analysis

Suitable single crystals of the ligand $\mathbf{HL^1}$ for X-ray diffraction measurements were obtained by slow evaporation of dilute alcoholic solution at room temperature. The X-ray diffraction data was collected on a Bruker KAPPA APEX II CCD diffractometer using Mo Kα radiation (λ = 0.71073 Å). Detailed procedures for cell refinement, data collection, and structural refinement were performed as described before.[2,20–25] The structure was solved by direct methods (SHELXS-97) and refined by full-matrix least-squares method based on F2 (SHELXL-97). The graphics interface program X-Seed was used for data presentation.[22] The crystallographic data of $\mathbf{HL^1}$ are presented in Table 2.

2.6 | Computational studies

All calculations were performed using Gaussian 09W software package. B3LYP/GENECP method using double-zeta plus polarization basis set 6-31G (d,p) for C, H, N, and O atoms and LANL2DZ basis set for the metal atoms was used to compute the geometries of the ligand and complexes. Quantum parameters such as electronegativity (χ), chemical hardness (η), electrophilicity, global softness, ionization potential, and electron affinity were estimated by using the HOMO and LUMO energies. Non-quantum parameters like the surface area grid (SAG), molar volume (MV), hydration energy (HE), polarizability (Pol), and molar refractivity (MR) were carried out using HyperChem 8.0.7. Natural bond orbital has been performed to measure the qualitative intermolecular delocalization in compounds. Total static dipole moment, (μ), mean polarizability (α), anisotropy of the polarizability ($\Delta\alpha$), and the mean first-order

TABLE 1 Color, yield, elemental analysis, mass spectrometry, and effective magnetic moment data for the reported compounds

Compound	Color	%Yield	Elemental analysis, found (calc.)			Mass spectrometry		μ_{eff} BM
			% C	% H	% N	Mol. wt.	Fragments (m/z)	
HL^1 $C_{15}H_{14}N_2O_2$	Brown	80	70.47 (70.85)	5.80 (5.55)	10.66 (11.02)	254.29	250, 254, 255	-
[Co(L^1)$_2$] $CoC_{30}H_{26}N_4O_4$	Orange	64	63.82 (63.72)	4.41 (4.63)	10.20 (9.91)	565.49	561, 562	3.45
[Ni(L^1)$_2$] $NiC_{30}H_{26}N_4O_4$	Faint green	70	63.56 (63.75)	4.81 (4.64)	9.73 (9.91)	565.26	560, 562	2.83
[Cu(L^1)$_2$]·2H$_2$O $CuC_{30}H_{30}N_4O_6$	Green	68	60.10 (59.45)	4.69 (4.99)	9.01 (9.24)	606.14	578, 593, 607	1.59
HL^2 $C_{16}H_{18}N_2O_3$	Yellow	80	67.04 (67.12)	6.38 (6.34)	9.66 (9.78)	286.33	269	-
[Ni(L^2)$_2$] $NiC_{32}H_{30}N_4O_4$	Faint green	62	64.73 (64.78)	5.10 (5.10)	9.17 (9.44)	593.31	591	2.62
HL^3 $C_{19}H_{16}N_2O_2$	Yellow	75	74.77 (74.98)	5.42 (5.30)	9.12 (9.21)	304.35	305	-
[Co(L^3)$_2$]·2H$_2$O $CoC_{38}H_{34}N_4O_6$	Reddish brown	73	65.33 (65.05)	4.52 (4.88)	8.13 (7.99)	701.64	694, 697, 698	3.27
[(NiL^3)$_2$] $Ni_2C_{38}H_{30}N_4O_4$	Faint green	68	62.89 (63.03)	3.88 (4.18)	7.57 (7.74)	724.08	675,720	2.45

hyperpolarizability (β) using the x, y, z components were calculated as reported in literature.[26]

2.7 | Biological activity studies

2.7.1 | Antibacterial activity

The **HL^1** ligand and its reported complexes were screened in vitro for their antibacterial activities using agar well diffusion method. Experimental details of the investigations are as described previously.[27] The antibacterial activities were scanned against two bacterial species: *Staphylococcus aureus* (gram positive) and *Escherichia coli* (gram negative). Ampicillin was used as a standard. Measurements were carried out in triplicate for each compound, and their average values are reported.

2.7.2 | Antioxidant assay (2,2-diphenyl-1-picrylhydrazyl free radical scavenging activity)

In vitro antioxidant activities of the reported complexes were evaluated using scavenging the stable 2,2-diphenyl-1-picrylhydrazyl (DPPH) radical method.[28] The radical scavenging test depends on the absorbance change of the radical when deactivated by antioxidants. Ascorbic acid was used as a standard compound. Stock solutions of the reported complexes were dissolved in methanol/DMSO (5:1) and then diluted to different concentrations. Detailed procedure for the DPPH free radical scavenging activity studies is previously given.[27]

2.7.3 | DNA-binding studies

The DNA-binding experiments of the complexes using calf thymus (CT-DNA) were carried out at room temperature. Detailed steps of the experiments are as described before.[27,29]

2.7.4 | Fluorescence quenching measurements

Studies of the competitive binding of DNA with ethidium bromide (EB) solution were carried out at different concentrations (1.0–8.0 $\times$ 10^{-5} M). The concentrations of EB and CT-DNA were kept constant (1.0 $\times$ 10^{-5} M for each). Before measurements, the resulting solutions were shaken up and incubated for 30 min. Details for the procedure and measurements are described previously.[27,30]

TABLE 2 Crystal structure data of the Schiff base ligand (**HL^1**)

Empirical formula	C15 H14 N2 O2
Formula weight	254.28
Temperature	120(2) K
Wavelength	1.54184 Å
Crystal system	Monoclinic
Space group	$P2_1/c$
Unit cell dimensions	a = 10.7596(3) Å b = 13.5263(4) Å c = 8.9645(3) Å α = 90° β = 100.047(3)° γ = 90°
Volume	1284.66(7) Å^3
Z	4
Density (calculated)	1.315 mg/m^3
Absorption coefficient	0.720 mm^{-1}
F(000)	536
Crystal size	0.326 × 0.281 × 0.131 mm^3
Theta range for data collection	4.173–76.854°
Index ranges	−11 < =h < =13 −17 < =k < =16 −11 < =l < =10
Reflections collected	8239
Independent reflections	2696 [*R*(int) = 0.0237]
Completeness to theta = 67.684°	99.8%
Absorption correction	Analytical
Max. and min. transmission	0.978 and 0.955
Refinement method	Full-matrix least squares on F^2
Data/restraints/parameters	2696/0/180
Goodness of fit on F^2	1.046
Final *R* indices [*I* > 2sigma(*I*)]	R1 = 0.0508, wR2 = 0.1423
R indices (all data)	R1 = 0.0527, wR2 = 0.1438
Extinction coefficient	n/a
Largest diff. peak and hole	0.278 and −0.232 e.Å^{-3}

2.7.5 | Viscosity measurements

Viscosity experiments were performed using Ostwald viscometer immersed in a water bath at a constant temperature. Samples of CT-DNA were prepared by sonication in order to reduce complexity arising from the CT-DNA flexibility. Flow time was measured three times for each sample, and the average was then calculated. Data were presented and estimated as described before.[2]

2.8 | Molecular docking studies

Molecular docking studies were performed using Molecular Operating Environment (MOE) software package version 2016.08. X-ray crystal structure of a B-DNA (dodecamer d [CGCGAATTCGCG]$_2$ running 3′–5′ direction, PDB ID: 1BNA) was used as a macromolecule target. Structure of the DNA was energetically optimized after inserting hydrogen atoms. The resulting model afforded to systematic conformational research with RMS gradient of 0.01 kcal mol^{-1}.

3 | RESULTS AND DISCUSSION

3.1 | Spectroscopic studies

The Schiff base ligand **HL^1** and the previously reported **HL^2** and **HL^3**[[2]] were synthesized by condensation of the appropriate amine and aldehyde derivatives (Scheme 1). Interaction of the Schiff bases **HL^1** and **HL^2** with M(II), M = Co(II), Ni(II), or Cu(II) ions gave coordination complexes with a general formula **[M(L)$_2$]**, except for **[Cu(L^1)$_2$]·2H$_2$O**, which was crystallized with two water molecules. On the other hand, cobalt(II) and nickel(II) derivatives of **HL^3** ligand have different structural arrangements (**[Co(L^3)$_2$]·2H$_2$O** and **[(NiL^3)$_2$]**). The structure of **HL^1** and the complexes was investigated by using different spectroscopic tools, such as FTIR, ^{1}H NMR, and mass, along with elemental analyses, magnetic measurements, molar conductivity, and thermal analysis. In addition, the structure of **HL^1** was elucidated by single-crystal X-ray diffraction technique. Elemental analyses and mass spectral data of the reported compounds were in accordance with the proposed molecular formulas. The molar conductivities of 1 × 10^{-3} M solutions of all complexes at 25°C were found to be in the range of 10–13 Ω^{-1} mol^{-1} cm^2, indicating that nonelectrolyte characteristics of these derivatives and the ligand anions are directly bonded to the M(II) centers neutralizing their charges. The effective magnetic moment (μ_{eff}) values calculated from the magnetic susceptibility measurements at 298 K are given in Table 1. Except for **[Ni(L^3)]$_2$**, the reported μ_{eff} values of the other complexes confirmed that they were mononuclear derivatives. The little deviation of the magnetic moment values from the spin-only values could be due to spin–orbit coupling. On the other hand, the binuclear nickel(II) derivative of **HL^3** gave an effective magnetic moment (μ_{eff}) value = 4.90 BM, that is, 2.45 BM for each Ni species. This value represents the spin-only value of two unpaired electrons for every nickel ion.

The infrared spectra (KBr pellets) of the ligand and complexes were performed in the wavenumber range of

4000–400 cm^{-1}. Important FTIR data for **HL¹** and the reported complexes are given in Table 3. The FTIR spectrum of the **HL¹** displayed stretching frequency bands at 3330, 3278, 3198, 1637, 1588, 1244, and 1075 cm^{-1}, which are assigned to υ(OH), υ(NH), υ(C=O), υ(C=N), υ(C–O), and υ(N–N), respectively.[2,27,31] Thus, the FTIR spectrum of the **HL¹** ligand in the solid state indicated that they existed in a keto form structure (Scheme 1). The ^{1}H NMR studies of **HL¹** in DMSO displayed a set of four slightly broad singlets at 9.04, 9.16, 10.04, and 11.18 ppm due to the protons of OH and NH groups. These signals were disappeared on the addition of D_2O (Figure 1). The line broadening of the four signals with comparable rates confirmed that the protons of the OH and NH groups are exchangeable, that is, the compound is fluxional at the NMR time scale. Therefore, **HL¹** existed in solution in two tautomeric (keto and enol) forms (Scheme 1).[32] The fact that **HL¹** exists in two isomers with a ratio of about 4:1 is also confirmed from the appearance of two signals for two CH=N (8.30 and 8.42 ppm) and two CH_2 (3.86 and 3.96 ppm). In addition, the ^{1}H NMR spectrum of **HL¹** exhibited multiplet signals corresponded to the aromatic protons (6.90–7.34 ppm). Interestingly, **HL²** (a similar derivative to **HL¹** with substitution of the azomethine proton by a methyl group; Scheme 1) was not fluxional at the NMR time scale, whereas **HL³** was fluxional.[2]

The FTIR spectra of the reported complexes exhibited the ligand bands with the appropriate shifts because of complex formation. The OH vibrational bands of the ligands disappeared from the FTIR spectra of the cobalt(II) and nickel(II) complexes. In the case of **[Cu(L¹)₂]·2H₂O** and **[Co(L³)₂]·2H₂O** complexes, new OH bands (3428 and 3443 cm^{-1}) appeared due to the water molecules. The shifts in the bands of the other functional groups, such as C=N, C=O, and C–O, toward low frequencies indicated that the ligands coordinated to metal ion from their O and N donor atoms.[2,27] All the reported complexes displayed new non-ligand bands for stretching frequencies of the M–O and M–N moieties due to

TABLE 3 Important FTIR data for the reported compounds

Compound	FTIR data, cm^{-1}						
	ν(OH)	ν(NH)	ν(C=O)	ν(C=N)	ν(C–O)	ν(M–O)	ν(M–N)
HL¹	3330(m) 3278(m)	3198(s)	1637(s)	1588(vs)	1244(m)	---	---
[Co(L¹)₂]	---	3198(s)	1589	1500	1187(m)	531(w)	492(w)
[Ni(L¹)₂]	---	3199(s)	1593(m)	1524(vs)	1195(m)	532(w)	478(w)
[Cu(L¹)₂]·2H₂O	3428(m)	3198(s)	1592(m)	1511(m)	1200(m)	532(w)	478(w)
[Ni(L²)₂]	---	3200(m)	1629(s)	1587(s)	1240(m)	528(w)	511(w)
[Co(L³)₂]·2H₂O	3443(m)	3194(m)	1615(s)	1600(s)	1188 (m)	524(w)	480(w)
[Ni(L³)]₂	---	---	---	1616(s) 1600(s)	1188 (m)	500(w)	483(w)

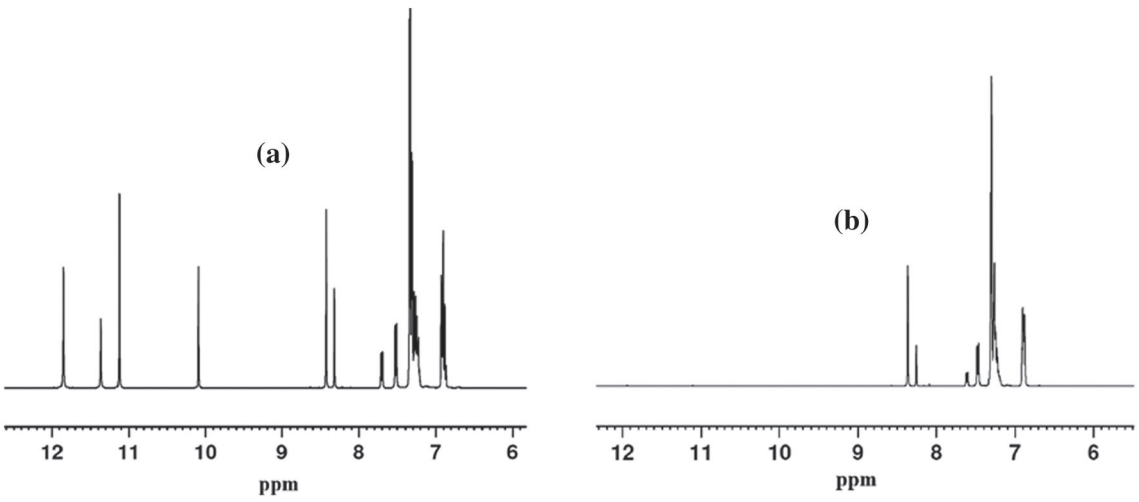

FIGURE 1 The ^{1}H NMR spectra of the Schiff base (**HL¹**): (a) in DMSO; (b) in DMSO + D_2O

complex formation[33] (Table 3). Figure 2 illustrates the proposed structures of the reported complexes. As can be noted, the ligands coordinated to the metal ions with the keto form, except for **[(NiL^3)$_2$]** complex, where the **HL^3** ligand bound to the metal with the enol form. Such behavior was previously observed in the copper dimer **[(CuL^3)$_2$]**.[2]

3.2 | X-ray crystallographic studies

The crystal structure of **HL^1** was determined by X-ray diffraction analysis. The data for the crystal structure of **HL^1** are deposited in Cambridge Crystallographic Data Center (see Supporting information). Accurate lattice parameters were determined from least-squares refinements of well-centered reflections in the range of $4.173° \leq \theta \leq 76.854°$. During data collection, three standard collections were periodically observed without significant intensity variations. The collected reflections were found to be 8239, whereas the independent reflections were 2696 with $I > 2{:}00\sigma(I)$. The observed reflections were used for structure determination and refinements. Ranges of h, k, and l for the ligand were $-11 \leq h \leq 13$, $-17 \leq k \leq 16$, $-11 \leq l \leq 10$. The crystallographic data for the ligand derivative are summarized in Table 2, and selected bond lengths and bond angles are given in Table 4. The crystallographic analysis showed that **HL^1** crystallized in monoclinic $P2_1/c$ space group with a Z value of 4. The ORTEP representation of **HL^1** ligand is given in Figure 3. The structure is nonplanar, and the molecule is completely unsymmetrical with a C_1 point group. The phenolic azomethine N–N and C=O moieties are almost in the same plane, although the benzyl part of the molecule is bent on the plane. The dihedral angles of C(1)–C(6)–C(7)–N(1) and N(1)–N(2)–C(8)–C(9) are 170.20° and 179.30°. On the other hand, the torsion angles of C(8)–C(9)–C(10)–C(15) and C(8)–C(9)–C(10)–C(11) are 79.73° and 76.53°. Also, the angles C(8)–N(2)–N(1), N(1)–C(7)–C(6), O(2)–C(8)–N(2), and O(2)–C(8)–C(9) have values around 120°. These values are corresponding to sp^2 hybridization and indicating that this part of molecule is nearly planar. The bond lengths of C(7)–N(1) in the imine group and N(1)–N(2) are 1.289 and 1.384 Å, respectively. These values are in the normal range of double and single bond separation.[34,35] These

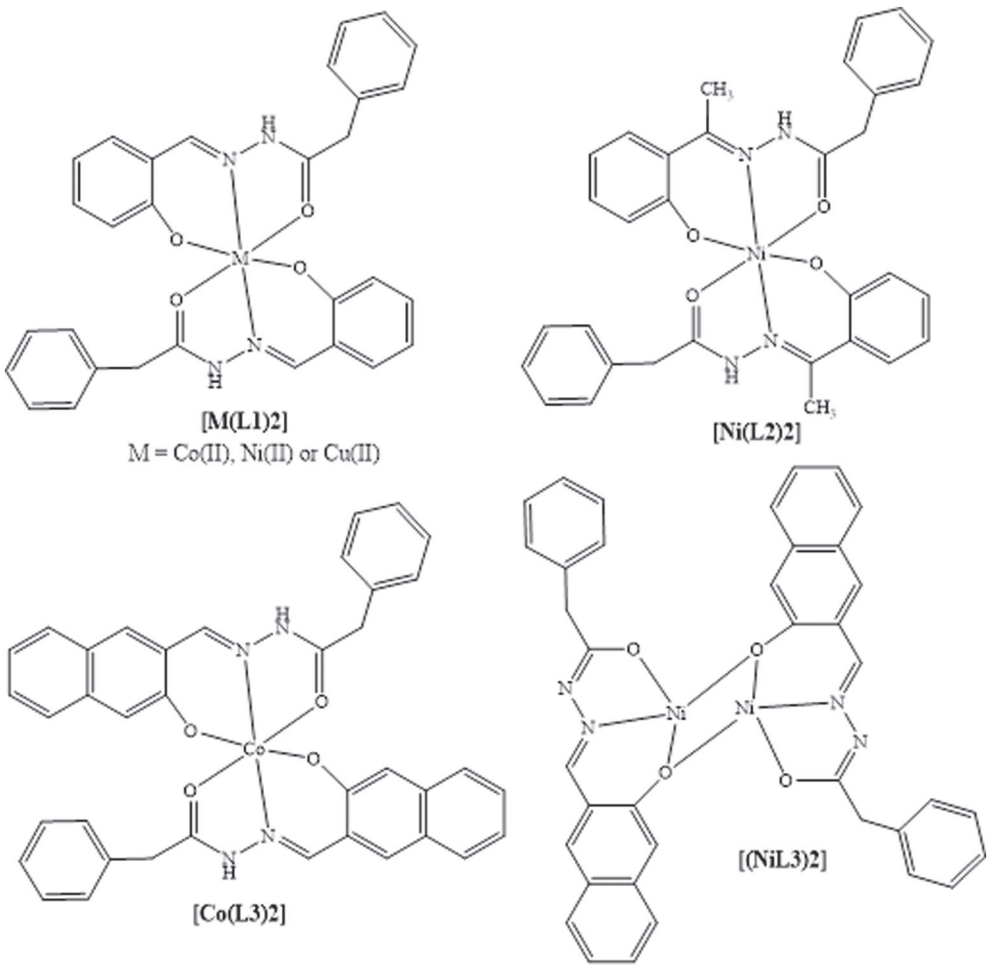

FIGURE 2 The proposed structures of the reported complexes

TABLE 4 Important bond lengths and angles for the Schiff base (**HL^1**) ligand

Bond lengths (Å)			
O(1)–C(1)	1.356(2)	O(2)–C(8)	1.227(2)
N(1)–C(7)	1.289(2)	N(1)–N(2)	1.3840(18)
N(2)–C(8)	1.340(2)	O(1)–H(1)	0.87(3)
C(6)–C(7)	1.456(2)	C(8)–C(9)	1.519(2)
Bond angles (°)			
C(1)–O(1)–H(1)	107.5(18)	C(7)–N(1)–N(2)	115.80(13)
C(8)–N(2)–N(1)	120.08(13)	O(1)–C(1)–C(2)	117.80(14)
O(1)–C(1)–C(6)	122.10(14)	O(2)–C(8)–N(2)	123.78(14)
O(2)-C(8)-C(9)	121.35(15)	C(10)–C(9)–C(8)	110.38(13)

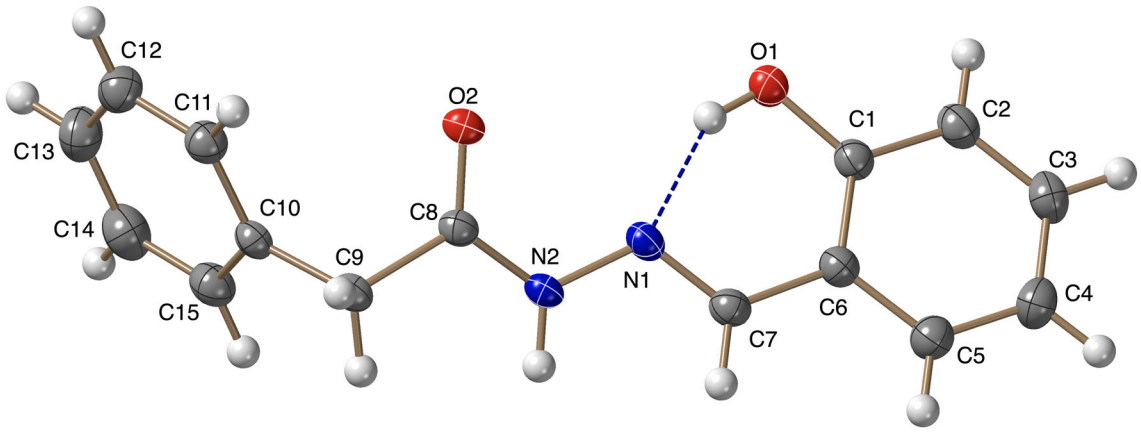

FIGURE 3 ORTEP diagram of the Schiff base (**HL^1**) ligand with 30% thermal ellipsoid

values are comparable with the values found for the ligand **HL^2** (1.2944 and 1.3723 Å), where the hydrogen of azomethine was substituted with a methyl group.[2] Furthermore, the C(8)–O(2) and C(1)–O(1) bond lengths are found to be 1.227 and 1.356 Å, which confirmed the presence of a double and a single bond characteristics for the two groups. All other bond lengths and bond angles are found in the normal ranges observed for similar compounds. Content of the unit cell of **HL^1** crystal showed that the molecules are connected to a net of hydrogen bonds (Figure 4). It showed the presence of intramolecular hydrogen bonding (O(1)–H(1)···N(1)) and intermolecular hydrogen bonding (N(2)–H(2)···O(2) and aromatic hydrogen atoms with oxygen of adjacent molecules). Table 5 illustrates the van der Waals displacement between H, the donor (D), and the acceptor (A) as well as the DHA angle.

3.3 | Thermal analysis

TG technique is very useful in confirming the composition and structure of the complexes. The thermal analysis studies of the complexes of **HL^1** ligand gave more information about the thermal stability of the metal complexes, the presence of hydrated water molecules, and the sequence of thermal decomposition. The TG plot of **[Co(L^1)$_2$]** displayed two overlapped decomposition steps and a well-defined and resolved step. The overlapped two decomposition steps occurred in the temperature range of 200–345°C with a net weight loss of 84.7% corresponding to elimination of most of organic moieties ($C_{28}H_{22}N_4O_4$). The second decomposition step occurred in the temperature range of 380–650°C with a weight loss of 5.2% and corresponded to the elimination of C_2H_4 moiety to give finally a metallic residue (10.1%). The thermal plot of **[Ni(L^1)$_2$]** exhibited four decomposition steps. The second and the third steps were overlapped. The first decomposition step occurred in the temperature range of 170–318°C with a net weight loss of 36.6% corresponding to elimination of $C_{10}H_{13}N_3O_2$ moieties. The second and third overlapped decomposition peak occurred in the temperature range of 320–380°C with a weight loss of 19.2% and corresponded to the material decomposition of C_6H_6NO species. The third resolved decomposition step existed in the

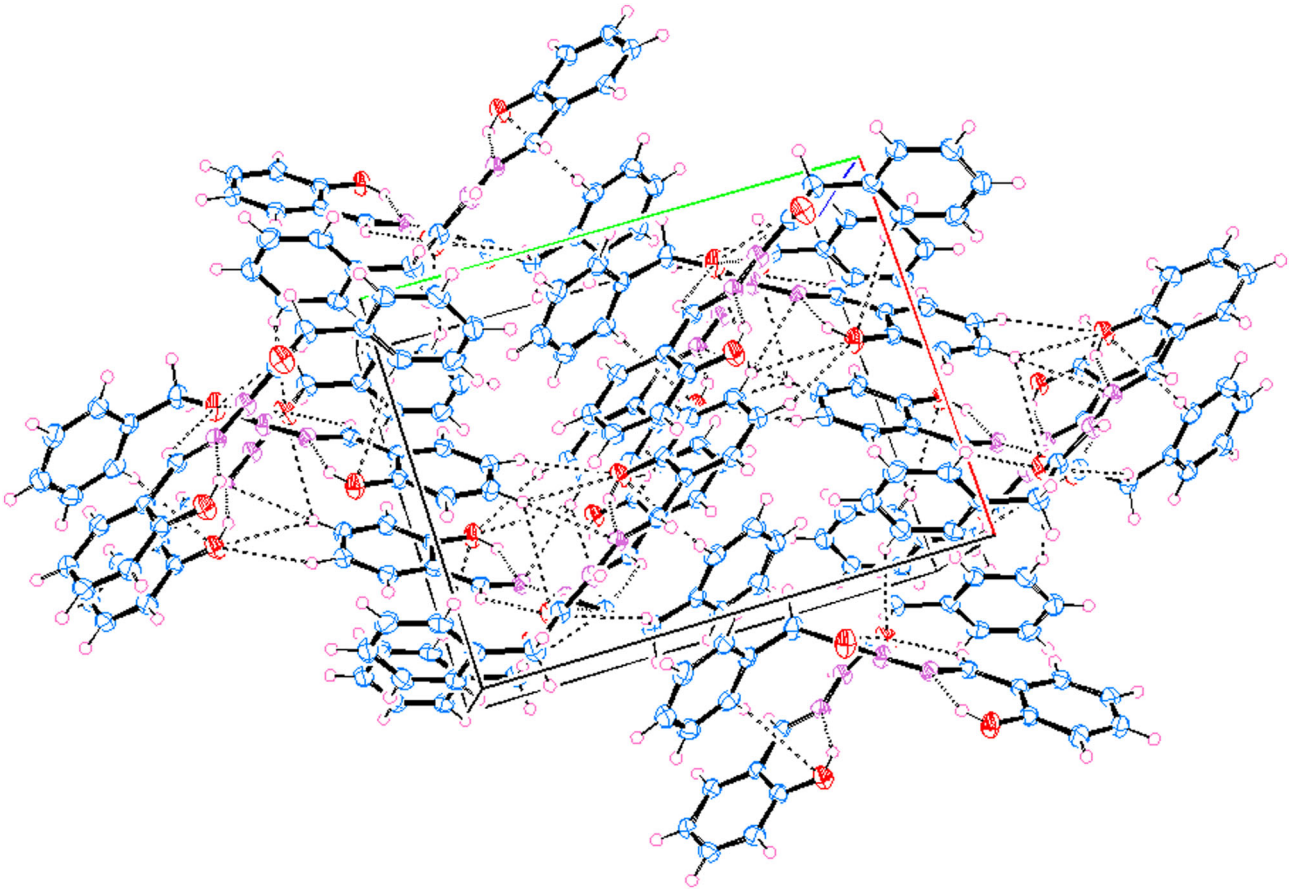

FIGURE 4 Unit cell packing diagram for the Schiff base (**HL^1**) ligand

TABLE 5 Hydrogen bonds for the Schiff base (**HL^1**) ligand

D–H···A	d(D–H) Å	d(H···A) Å	d(D···A) Å	<(DHA)°
O(1)–H(1)···N(1)	0.87(3)	1.85(3)	2.6279(17)	148(3)
N(2)–H(2)···O(2)	0.90(2)	1.85(2)	2.7304(17)	166(2)

temperature range of 380–825°C with a weight loss of 26.5% corresponding to the elimination of $C_{12}H_7$ species to afford the residue NiC_2 + O (17.7%). The TG plot of **[Cu(L^1)$_2$]·2H$_2$O** displayed two overlapped and two well-resolved decomposition steps. The overlapped first and second decomposition steps occurred in the temperature range of 100–295°C with a net weight loss of 27.1% corresponding to elimination of $2H_2O + C_8H_6N_2$ species. The second decomposition peak occurred in the temperature range of 295–518°C with a weight loss of 44.9% and corresponded to the material decomposition of $C_{17}H_{10}N_2O_2$ moieties. The third decomposition step occurred in the temperature range of 518–1000°C with a weight loss of 13.9% corresponding to the elimination of $C_5H_{10}O$ species and yielded a copper oxide residue. From the thermal data, it was confirmed that the copper complex crystallized with two water molecules. In addition, it can indicate that the thermal stability of the complexes has the order **[Cu(L^1)$_2$]·2H$_2$O** > **[Co(L^1)$_2$]** > **[Ni(L^1)$_2$]**.

3.4 | Molecular orbital computation of HL^1 and its complexes

3.4.1 | Geometrical optimization of HL^1 and its complexes

Optimized geometrical parameters, natural charges on the active centers, natural configuration of the metal ions, and energetics of the ground state for the studied compounds were computed using density functional theory (DFT) method at the B3LYP/GENECP level of theory. The ligand **HL^1** was found to exist in solution in two geometrical structures, namely, the keto and enol forms (see above, Scheme 1). Therefore, both the two structures

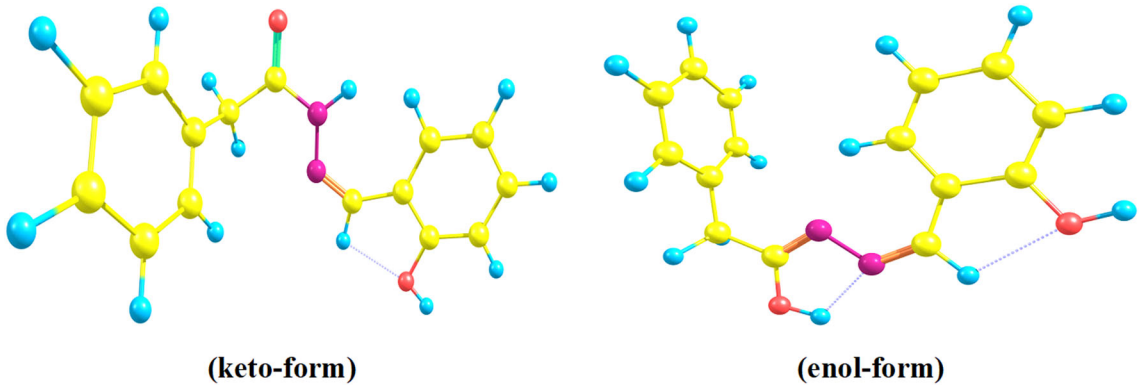

FIGURE 5 The optimized geometry of the Schiff base (**HL^1**) ligand in its two tautomeric forms

TABLE 6 The energetics and partial charge of active centers of the tautomers of **HL^1** and its anion

	HL^1 (keto)	HL^1 (enol)	L$_1^-$
E_T, au	−840.181	−840.176	−839.652
E_{HOMO}, au	−0.00187	−0.00716	−0.05378
E_{LUMO}, au	0.00622	0.00123	0.05921
E_g (eV)	0.220	0.228	3.073
O_9	−0.60694	−0.67835	−0.65785
O_{18}	−0.67532	−0.69195	−0.80907
N_{10}	−0.43341	−0.46906	−0.39155
N_{11}	−0.25259	−0.36564	−0.33074
μ, D	5.7148	2.899	9.9646

(keto/enol) were considered for optimization. The optimized geometry of **HL^1** in the two tautomeric forms is shown in Figure 5. The energetics of the ligand and natural charges are listed in Table 6.

The observed data indicated that the keto form is more stable than the enol form by ∼12 kcal mol^{-1} as reflected from the calculated total energy. These data are confirmed by the experimental finding. It is clear that the natural charges calculated from the NBO analysis showed that the most negative centers for chelation are the two oxygen and adjacent nitrogen atoms (O9, O18, and N11). In addition, the anion form of the ligand was considered for optimization using the same level of theory. It was found that the natural charges on (O9, O18, and N11) in **L$_1^-$** are greater than that in **HL^1**. By comparing the data of the anion and the keto form of the ligand, it can be concluded that the anion is the favorite moiety for the complexation process. This could be due to the higher dipole moment for **L$_1^-$**, which is higher than the dipole moment of **HL^1** itself. The higher dipole moment usually indicates higher polarity and higher tendency to react with other charged species.

The optimized structures, numbering system, the vectors of dipole moment, bond lengths, and bond angles of the three complexes of **HL^1** (**[Cu(L^1)$_2$]**, **[Co(L^1)$_2$]**, and **[Ni(L^1)$_2$]**) are presented in Figure 6. In these complexes, the metal ions are in octahedral environment and coordinated to two ligands, each with a five-membered ring and a six-membered ring. The computed M–N and M-–O bond lengths showed elongation upon complexation. The bonds between M and ligand sites in **[Cu(L^1)$_2$]·2H$_2$O**—for example, Cu44–N2 = 2.029 Å, Cu44–O9 = 2.103 Å, Cu44–O43 = 2.299 Å, Cu44–N23 = 2.012 Å, Cu44–O30 = 2.014 Å, and Cu44–O62 = 2.429 Å—and the bond angles between the metal species and the binding sites in the coordination sphere vary between 76.16° and 103.35°. The bonds between M and ligand sites in the case of **[Ni(L^1)$_2$]** are Ni44–N2 = 1.912 Å, Ni44–O9 = 1.935 Å, Ni44–O43 = 2.459 Å, Ni44–N23 = 1.945 Å, Ni44–O30 = 2.250 Å, and Ni44–O62 = 2.094 Å. The bond angles between the metal species and the binding sites in the coordination sphere varied between 80.51° and 98.77°. On the other hand, the bonds between M and ligand sites in **[Co(L^1)$_2$]** are Co44–N2 = 2.019 Å, Co44–O9 = 2.008 Å, Co44–O43 = 2.141 Å, Co44–N23 = 2.037 Å, Co44–O30 = 2.056 Å, and Co44–O62 = 2.098 Å, and the bond angles between the metal ion and binding sites in the coordination sphere vary between 79.11° and 104.64°. The calculated dihedral angles around the metal in the coordination sphere for the three complexes were far from 0° or 180°. This revealed that the metal species is not in the same plane of the donating sites and the rest of the ligand, that is, the complexes, are not planar.

3.4.2 | Natural charge and natural population of HL^1 and its complexes

The accumulation of charges on the individual atoms coordinated with the metal ion before and after

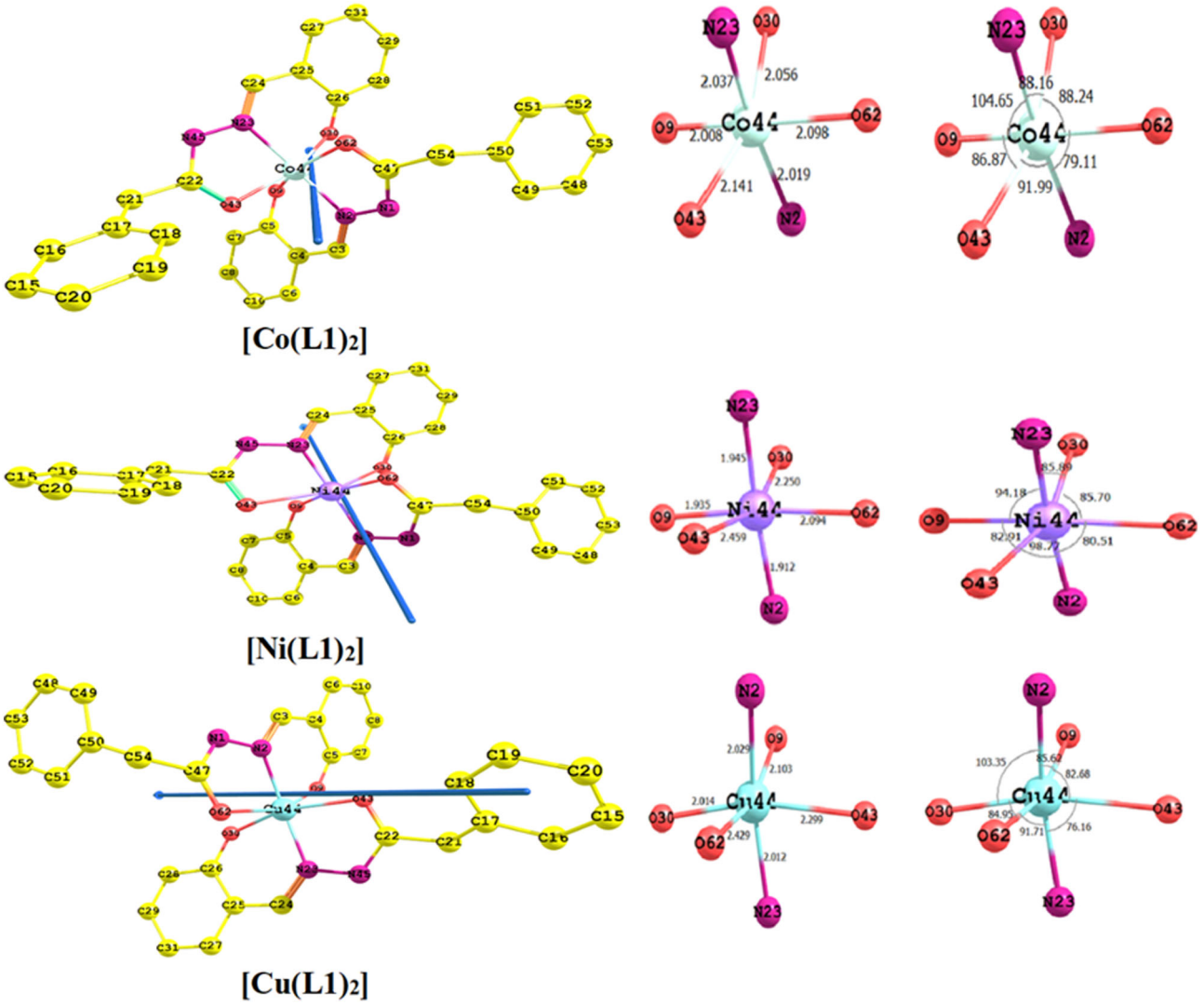

FIGURE 6 Optimized structures of the Schiff base (**HL^1**) complexes

TABLE 7 Natural charge and natural population of complexes of **HL^1**

Complex	Natural charge	Natural population			Natural electronic configuration
		Core	Valence	Rydberg	Total	
[Co(L^1)$_2$]	−0.08492	8.99746	4.57907	0.00839	13.58492	[core]4s(0.13), 3d(4.22), 4p(0.08), 5p(0.15)
[Ni(L^1)$_2$]	0.68974	17.99440	9.30110	0.01476	27.31026	[core]4s(0.27), 3d(8.59), 4p(0.44), 5p(0.01)
[Cu(L^1)$_2$]	0.41134	17.99665	10.58103	0.01099	28.58866	[core]4s(0.26), 3d(9.90), 4p(0.42), 5p(0.01)

complexation, natural population of electrons of each metal ion in the core, valence and Rydberg subshells, and natural electronic configuration of metal ions in the coordination globe of the complexes of **HL^1** ligand are given in Tables 7 and 8. The most electronegative charges existed on O9, O18, and N11 atoms of the ligand and complexes. Thus, these electronegative atoms in the coordination sphere have a tendency to provide electrons to the central metal. On the other hand, the most electropositive charges are centered on the Cu(II), Ni(II), and Co(II) ions. Such atoms are more able to receive electrons from the ligands. In **[Cu(L^1)$_2$]** complex, the Cu central ion receives 1.5886e from the ligand with $3d^{9.90}$ configuration. In the case of **[Ni(L^1)$_2$]** complex, the Ni ion receives 1.3102e from the ligand with $3d^{8.59}$ configurations. In the case of **[Co(L^1)$_2$]** complex, the Co ion receives 1.9150e from the ligand with $3d^{4.22}$ configurations.

3.4.3 | Quantum global reactivity descriptors of HL^1 and its complexes

The global reactivity descriptors of **HL^1** anion and its complexes—HOMO and LUMO, energy gap (*Eg*), electronegativity(χ), chemical potential (*V*), electron affinity (*A*), ionization potential (*I*), chemical hardness (η), and chemical softness (*S*)—are presented in Table 9. The *Eg* separation between the HOMO and LUMO of the complexes characterizes the molecular chemical reactivity. The smaller energy gap reflects the ease of the charge transfer and polarization within the compound. The donating properties, E_{HOMO}, of the complexes follow the order **[Ni(L^1)$_2$] > [Co(L^1)$_2$] > [Cu(L^1)$_2$]**, whereas the accepting properties, E_{LUMO}, follow the order **[Cu(L^1)$_2$] > [Co(L^1)$_2$] > [Ni(L^1)$_2$]**. Thus, the order of increasing chemical reactivity follows the order **[Ni(L^1)$_2$] > [Co(L^1)$_2$] > [Cu(L^1)$_2$]**. From the HOMO and LUMO energies, ionization potential and electron affinity are expressed as $I \sim -E_{HOMO}$ and $A \sim -E_{LUMO}$. The variations in electronegativity (χ) values is sustained by the electrostatic potential. The results showed that the order of decreasing electronegativity, that is, increasing charge transfer within the complexes, is **[Co(L^1)$_2$] < [Cu(L^1)$_2$] < [Ni(L^1)$_2$]**. Smaller η values for the complexes imitated the ability of charge transfer inside the molecules. The order of increasing charge transfer within the complexes is **[Ni(L^1)$_2$] > [Co(L^1)$_2$] > [Cu(L^1)$_2$]**.

3.4.4 | Non-quantum global reactivity descriptors for HL^1 anion and its complexes

The calculated values of the physicochemical properties of **HL^1** anion and its complexes are given in Table 10. The considered computed parameters are *MV*, *HE*, *Pol*, *SAG*, and *MR*. Calculations were carried out using HyperChem 8.0.7. Molecular polarizability (*Pol*) characteristics is defined by the capacity of the electronic system of a molecule to modulate itself upon application of external electric field of light. The meaning of molecular polarizability stems from its important role in the modeling of many biological activities and properties of molecules. Molecular polarizability depends on the molecular volume that determines the transport characteristics of molecules. In biological environment, for example, it

TABLE 8 Natural charge on the coordinated centers of complexes of **HL^1**

Center	L_1^-	[Co(L^1)$_2$]	[Ni(L^1)$_2$]	[Cu(L^1)$_2$]
O_9	−0.64616	−0.31398	−0.61766	−0.64282
O_{18}	−0.80601	−0.35196	−0.65704	−0.70447
N_{11}	−0.31956	−0.14734	−0.31553	−0.28104
O_9	−0.64616	−0.33557	−0.57997	−0.52073
O_{18}	−0.80601	−0.29596	−0.60224	−0.58300
N_{11}	−0.31956	−0.13884	−0.31105	−0.28896

TABLE 10 Non-quantum global parameters of **HL^1** anion and its complexes

Parameter	L_1^-	[Co(L^1)$_2$]	[Ni(L^1)$_2$]	[Cu(L^1)$_2$]
SAG, Å^2	451.08	762.54	761.57	761.57
MV, Å^3	724.06	1409.22	1407.63	1407.63
Log P	1.84	1.91	1.91	1.91
HE, kcal mol^{-1}	−6.28	−14.64	−14.48	−14.41
Pol, Å^3	81.09	55.45	55.46	55.47
MR, Å^3	81.09	160.40	160.40	160.40
MW, amu	253.28	565.49	565.27	570.11

TABLE 9 Quantum global properties of **HL^1** anion and its complexes

Parameter	L_1^-	[Co(L^1)$_2$]	[Ni(L^1)$_2$]	[Cu(L^1)$_2$]
E_T, au	−839.652	−1823.863	−1848.078	−1874.710
E_{HOMO}, au	−0.05378	−0.15788	−0.15617	−0.17609
E_{LUMO}, au	−0.05921	−0.05171	−0.07707	−0.04979
E_g, eV	3.073	2.8878	2.1515	3.4353
I, eV	1.4628	4.2943	4.2478	4.7896
A, eV	−1.6105	1.4065	2.0963	1.3542
χ, eV	−0.0738	2.8504	3.1720	3.0719
η, eV	1.5366	1.4439	1.0757	1.7177
S, eV	0.3253	0.3462	0.4648	0.2910
V, eV	−2.2679	−4.1124	−3.1996	−3.5910

includes blood–brain barrier penetration and intestinal absorption.[36] Thus, the modeling of molecular properties and biological properties need the use of molecular volume in the quantitative structure–activity relationships. Molar refractivity is a steric parameter, and it depends on the spatial array of the aromatic rings in molecules. The significance of the spatial arrangement is essential to study the interaction of drug molecules with the receptors.[37] It also depends on the London dispersive forces, which play a strong role in drug molecule–receptor interactions. Table 10 illustrates that the polarizability data, MR, and SAG are mostly proportional to the size and molecular weight of the reported complexes. The data also show that the hydration energy increases because of increasing the hydrophobic values. The number of hydrogen bonds between acceptor and donor affects the change in the values of the hydration energy.[38]

3.4.5 | Nonlinear optical properties of HL^1 anion and its complexes

In order to determine the relationship between molecular structure and nonlinear optical (NLO) properties, the polarizabilities and hyperpolarizabilities of the reported complexes of **HL^1** were calculated. Total static dipole moment (μ), mean polarizability (α), anisotropy of polarizability ($\Delta\alpha$), and the mean of first-order hyperpolarizability (β) of the ligand and its complexes are listed in Table 11. The polarizabilities and first-order hyperpolarizabilities are given in atomic units (au). The calculated values for α and β have been converted into electrostatic units (esu) using conversion factors (0.1482×10^{-24} esu for α and 8.6393×10^{-33} esu for β). Urea was used as a standard prototype in the NLO studies.[39] The magnitude of β is one of the key factors in a NLO system. The theoretical analysis of β for **HL^1** and its complexes showed that both the **L_1^-** and **$[Co(L^1)_2]$** are

TABLE 11 Nonlinear optical properties of **HL^1** anion and its complexes

Parameter	L_1^-	$[Cu(L^1)_2]$	$[Ni(L^1)_2]$	$[Co(L^1)_2]$
μ_x	−4.8227	−3.4470	0.3091	−1.7541
μ_y	3.3344	0.3430	0.8638	−1.4928
μ_z	0.3517	2.8755	5.6883	8.5677
μ, D	5.8736	4.50199	5.76177	8.87191
α_{xx}	−155.4734	−199.1806	−194.9582	−198.7639
α_{yy}	−156.5369	−183.5469	−210.3597	−199.8309
α_{zz}	−117.1237	−228.1542	−223.9595	−242.5692
α_{xy}	16.5974	−13.6887	−16.5676	−25.6764
α_{xz}	3.1031	7.2178	−24.5580	6.4472
α_{yz}	−0.3168	−3.9854	10.4222	−0.1726
α, au	−143.044	−203.627	−209.759	−213.721
α, esu	-2.119×10^{-23}	-3.017×10^{-23}	-3.108×10^{-23}	-3.167×10^{-23}
$\Delta\alpha$, au	21.1386	39.2026	25.13201	43.28166
β_{xxx}, au	−28.6122	−9.4458	−32.9232	14.1877
β_{yyy}	−21.8399	38.4135	62.2989	7.2048
β_{zzz}	0.9351	−20.0290	42.6708	46.1826
β_{xyy}	−32.8975	−1.8560	−0.5201	−12.2676
β_{xxy}	76.3865	64.3180	−18.8236	13.7234
β_{xzz}	−13.6388	−58.8046	44.1482	−39.8389
β_{xxz}	−12.2361	−23.5458	5.9723	30.7659
β_{yzz}	7.7621	−31.8397	11.4005	−12.1919
β_{yyz}	0.3675	−29.7298	−4.4493	7.6161
β_{xyz}	−5.6705	−10.1743	−27.0125	19.0636
β, au	98.230	123.750	69.446	93.060
β, esu	8.486×10^{-31}	1.069×10^{-30}	5.999×10^{-31}	8.039×10^{-31}

fourfold greater than urea. However, the **[Ni(L^1)$_2$]** and **[Cu(L^1)$_2$]** complexes are threefold and fivefold greater than urea. These findings confirmed that the reported complexes are effective NLO candidates.

3.5 | Molecular orbital computations of the complexes of HL^2 and HL^3

3.5.1 | Geometrical optimization of the complexes

The geometrical optimizations of the two ligands **HL^2** and **HL^3** were previously reported.[2] The optimized structural geometry, numbering, dipole moment, bond lengths, and bond angles of the complexes of **HL^2** and **HL^3** are shown in Figure 7. In **[Ni(L^2)$_2$]** complex, the metal ion coordinated to two ligands, each forming a five- membered ring, namely, Ni21–O9-C8–N10–N11, and a six-membered ring, Ni21–N11–C12-C14–C19–O20, forming a distorted octahedral structure. The computed M–N and M–O bond lengths showed elongation upon complexation.[2] These bond lengths are much longer compared with the typical MX bond lengths (X = O or N).[40] The bonds between M and ligand sites in **[Ni(L^2)$_2$]** are Ni21–N22 = 2.076 Å, Ni21–O33 = 2.647 Å, Ni21–O20 = 1.867 Å, Ni21–N11 = 1.979 Å, Ni21–O41 = 2.010 Å, and Ni21–O9 = 1.971 Å. On the other hand, the bond angles between the nickel(II) ion and binding sites in the coordination sphere vary between 68.98° and 126.68°. The calculated dihedral angles around the metal species in the coordination sphere were far from 0° or 180° and revealed that the complexes is nonplanar.

The optimized structure of **[Co(L^3)$_2$]** complex exhibited a distorted octahedral structure similar to that of **[Co(L^1)$_2$]** and **[Ni(L^2)$_2$]** complexes (Figures 6 and 7). The bonds between Co and ligand sites are Co24–N11 = 1.965 Å, Co24–O9 = 2.064 Å, Co24–O25 = 1.834 Å, Co24–N37 = 1.928 Å, Co24–O40 = 1.848 Å, and Co24–O23 = 1.874 Å. In addition, the bond angles between cobalt ion and binding sites in the coordination sphere vary between 79.04° and 93.17°. In the case of **[(NiL^3)$_2$]** complex, the spectroscopic and analytical studies showed that it has a dinuclear structure similar to that observed for **[(CuL^3)$_2$]** complex.[2] The bonds between Ni and ligand coordination sites were found to have the following values: Ni24–N11 = 1.871 Å, Ni24–O9 = 1.878 Å, Ni24–O39 = 1.884 Å, Ni24–O23 = 2.075 Å, Ni40–N44 = 1.847 Å, Ni24–O47 = 1.854 Å, Ni24–O39 = 1.945 Å, and Ni24–O23 = 1.927 Å. The bond angles between Ni ion and the binding sites in the coordination sphere varied between 77.51° and 108.01°. The dihedral angles around the cobalt(II) and nickel(II) ions in the two complexes confirmed the nonplanarity conformation of their structure.

3.5.2 | Natural charge and natural population for the complexes of HL^2 and HL^3

The accretion of charges on the individual atoms coordinated with the metal ion before and after complexation, valence and Rydberg subshells, natural population of the electrons of each metal ion in the core, and natural electronic configuration of the metal ions in the coordination sphere of the **HL^2** and **HL^3** complexes are tabulated in Tables 12 and 13. The most electronegative charges are cumulated on N11, O9, and O18 atoms of the ligands and the complexes. These electronegative atoms in the coordination globe have, thus, a tendency to give electrons to the central metal ions. The most electropositive charges accrued on the Co(II) and Ni(II) species. Such atoms are more likely to receive electrons from the ligands. In the case of **[Ni(L^2)$_2$]**, the nickel(II) central metal ion receives 1.2881e from the ligand with 3d$^{8.56}$ configuration (Table 12). Again, the most electropositive charges accrued on the Co(II) and Ni(II) ions. Such atoms are more likely to receive electrons from the ligands. In the case of **[Co(L^3)$_2$]** complex, the Co central metal ion receives 1.4175e from the ligand with 3d$^{7.65}$ configurations. For the **[(NiL^3)$_2$]** complex, the two Ni central metal ions receive 1.24916e and 1.31859e from the ligand with 3d$^{8.65}$ and 3d$^{8.71}$configurations. In addition, there is an electron back-donation in the case of **[(NiL^3)$_2$]** from Ni to N11 and N11 of the other ligand by 0.00754 and 0.0163, respectively.

3.5.3 | Quantum global reactivity descriptors for the complexes of HL^2 and HL^3

The global properties of the complexes of **HL^2** and **HL^3** are presented in Table 14. The donating properties, E_{HOMO}, of the complexes follow the order **[Co(L^3)$_2$]** > **[Ni(L^2)$_2$]** > **[(NiL^3)$_2$]**, whereas the accepting properties, E_{LUMO}, are **[Ni(L^2)$_2$]** > **[Co(L^3)$_2$]** > **[(NiL^3)$_2$]**. From the energy gap (*Eg*), the order of increasing reactivity follows the order **[Co(L^3)$_2$]** > **[Ni(L^2)$_2$]** > **[(NiL^3)$_2$]**. The variation of electronegativity (χ) values is sustained by electrostatic potential. Table 14 shows that the order of decreasing χ (increasing charge transfer within the complexes) is **[Co(L^3)$_2$]** < **[Ni(L^2)$_2$]** < **[(NiL^3)$_2$]**. The ability of charge transfer inside the complexes (η) follows the order **[Co(L^3)$_2$]** > **[Ni(L^2)$_2$]** > **[(NiL^3)$_2$]**.

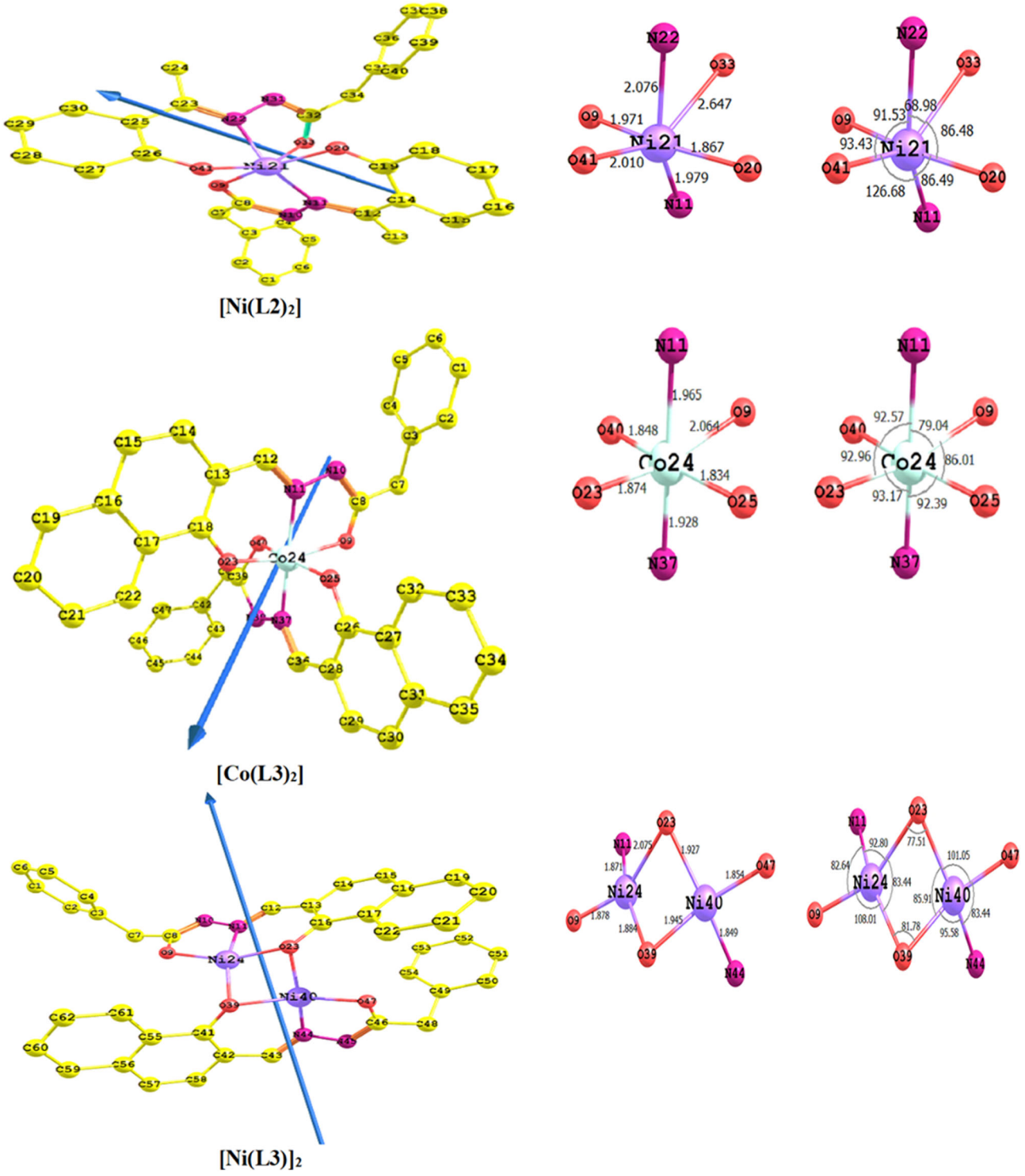

FIGURE 7 Optimized geometries, numbering system, vectors of dipole moment, bond lengths, and bond angles of the complexes of **HL²** and **HL³**

3.5.4 | Non-quantum global reactivity descriptors for the complexes of HL^2 and HL^3

The polarizability data, MR, and SAG are found to be proportional to the size and the molecular weight of the complexes (Table 15). In addition, the data showed that an increase in the hydrophobic values would result in an increase in the hydration energy. It is well known that the number of hydrogen bonds between acceptor and donor within the molecule affects the change in the values of hydration energy.[38]

TABLE 12 Natural charge and natural population of complexes of **HL²** and **HL³**

Complex	Natural charge	Natural population				Natural electronic configuration
		Core	Valence	Rydberg	Total	
[Ni(L²)₂]	0.71190	17.99483	9.27887	0.01440	27.28810	[core]4s(0.26)3d(8.56) 4p(0.01) 5p(0.46)
[Co(L³)₂]	0.58245	17.99009	8.40450	0.02297	26.41755	[core]4s(0.26) 3d(7.65) 4p(0.50) 4d(0.01) 5p(0.01)
[(Ni$_{(24)}$L³)₂]	0.75084	17.98753	9.25293	0.00870	27.24916	[core]4s(0.28) 3d(8.65) 4p(0.21) 5p(0.11)
[(Ni$_{(40)}$L³)₂]	0.68141	17.98763	9.32175	0.00920	27.31859	[core]4s(0.28) 3d(8.71) 4p(0.09) 5p(0.24)

TABLE 13 Natural charge on coordinated centers of complexes of **HL²** and **HL³**

Center	L_2^-	[Ni(L²)₂]	[Co(L³)₂]	[(NiL³)₂]
O_9	−0.64846	−0.56094	−0.59271	−0.64240
O_{18}	−0.80606	−0.62359	−0.63307	−0.71358
N_{11}	−0.36071	−0.29566	−0.25903	−0.32710
M → L	--	--	--	0.00754
O_9	−0.64846	−0.64558	−0.59885	−0.64240
O_{18}	−0.80606	−0.68267	−0.63523	−0.69748
N_{11}	−0.36071	−0.32052	−0.24866	−0.33586
M → L	--	--	--	0.0163

TABLE 14 Quantum global properties of **HL²** and **HL³** anions and their complexes

Parameter	L_2^-	[Ni(L²)₂]	L_3^-	[Co(L³)₂]	[(NiL₃)₂]
E_T, au	−878.978	−1926.703	−993.331	−2130.834	−2323.201
E_{HOMO}, au	−0.05072	−0.15135	−0.06098	−0.12427	−0.21217
E_{LUMO}, au	0.05822	−0.07093	−0.05980	−0.07813	−0.11718
E_g, eV	2.963	2.1874	0.2850	1.2550	2.5837
I, eV	1.3795	4.11672	1.6586	3.3801	5.7710
A, eV	−1.5835	1.92929	−1.6265	2.1251	3.1872
χ, eV	−0.102	3.023005	0.0160	2.7526	4.4791
η, eV	1.4815	1.093715	1.6425	0.6275	1.2919
S, eV	0.3374	0.45715	0.3044	0.7968	0.38702
V, eV	−2.1712	−3.023005	−0.9718	−2.3175	−4.1773

3.5.5 | NLO properties for the complexes of HL² and HL³

Analysis of the computed values of β for the ligands and complexes showed that **L_2^-** anion is six times greater than urea, whereas that of **L_3^-** anion is four times greater. On the other hand, the β values for **[Ni(L¹)₂]**, **[Co(L³)₂]**, and **[(NiL³)₂]** are nine, six, and five times greater than urea, respectively. These values confirmed the effectiveness of the complexes as NLO candidates. The result also showed that the NLO properties increased after complexation (Table 16).

3.6 | Biological activity studies

3.6.1 | Antibacterial activity

Antibacterial activities of the **HL¹** ligand and its complexes were screened in vitro against two bacteria, *E. coli* (gram negative) and *S. aureus* (gram positive), and compared with the known antibiotic: ampicillin as an antibacterial drug. The results indicated that all the complexes, except for the copper(II) derivative, have medium antibacterial activities with respect to that of standard (Table 17). The copper(II) complex has almost equal

TABLE 15 Non-quantum global properties of the complexes of **HL²** and **HL³**

Parameter	L_2^-	$[Ni(L^2)_2]$	L_3^-	$[Co(L^3)_2]$	$[(NiL_3)_2]$
SAG, Å²	464.24	810.30	545.20	886.17	892.29
MV, Å³	767.63	1480.94	902.32	1649.65	1660.84
Log P	2.80	3.82	1.91	2.06	2.56
HE, kcal mol⁻¹	−5.03	−12.31	−7.22	−14.06	−13.86
Pol, Å³	29.99	59.13	34.33	67.82	67.22
MR, Å³	85.56	169.35	99.28	196.79	192.89
MW, amu	267.31	593.32	303.34	665.61	722.08

TABLE 16 Nonlinear optical properties of the complexes of **HL²** and **HL³**

Parameter	L_2^-	$[Ni(L^1)_2]$	L_3^-	$[Co(L^3)_2]$	$[(NiL_3)_2]$
μ_x	−6.2423	−4.9746	−3.9297	−1.2278	−0.2220
μ_y	0.6129	−6.3278	−4.4312	−5.4425	0.9511
μ_z	−1.5332	−3.7867	−2.0088	−0.5475	−0.0163
μ, D	6.4569	8.89532	6.25406	5.60607	0.976801
α_{xx}	−165.8107	−191.0098	−168.3159	−226.8709	−251.4181
α_{yy}	−157.5241	−245.5255	−170.4271	−268.1970	−273.3155
α_{zz}	−129.1993	−232.1840	−144.2745	−260.2305	−281.4643
α_{xy}	16.4126	5.5998	−4.9223	12.8561	21.7355
α_{xz}	−4.3566	−8.4255	5.5405	−26.8051	−7.3279
α_{yz}	0.7243	−11.7620	7.3209	−3.5975	−1.7683
α, au	−150.844	−222.906	−161.005	−251.766	−268.732
α, esu	-2.235×10^{-23}	-3.303×10^{-23}	-2.386×10^{-23}	-3.731×10^{-23}	-3.982×10^{-23}
$\Delta\alpha$, au	33.2517	341.2284	25.1635	37.9748	26.9135
β_{xxx}, au	−104.0948	−122.5740	−58.8850	−15.7478	−27.5311
β_{yyy}	−59.7630	−28.0939	−71.5709	−95.5321	90.6218
β_{zzz}	19.8294	−18.7025	−12.0768	2.6856	44.9645
β_{xyy}	−17.0150	−45.6772	−25.5541	−53.1361	2.8666
β_{xxy}	67.7049	−62.2953	34.3919	−27.5208	−31.2332
β_{xzz}	−7.5757	18.5961	−19.1640	35.3874	25.3993
β_{xxz}	−18.9820	−11.6121	37.0768	9.6918	82.2592
β_{yzz}	7.2446	−38.9327	21.5118	−8.1829	−1.1774
β_{yyz}	−29.6504	−1.1085	−22.3486	−22.6376	−34.4865
β_{xyz}	11.6346	−24.7459	−0.8195	67.6481	−45.7672
β, au	132.740	200.270	104.814	135.831	109.495
β, esu	1.146×10^{-30}	1.730×10^{-30}	9.055×10^{-31}	1.173×10^{-30}	9.459×10^{-31}

activity similar to that of ampicillin. Therefore, coordination of Cu(II) ion to the ligand greatly enhanced the antibacterial activity. The activity of the ligand and complexes can be demonstrated by the cell permeability concept and/or Tweedy's chelation theory.[41–43] Due to the high polarity of metal ions, the cell permeability concept declared that these ions can hardly pass through the membrane, which surrounds the cell. On chelation, the polarity of the metal ions is significantly reduced as a result of the overlap of ligand and metal orbitals. Such overlap will lead to a partial contribution of the positive charge of metal ion with the donor groups. Furthermore, the lipophilicity of copper(II) complex is improved as the π-electron delocalization over the whole chelating ring increases. Subsequently, the penetration of the complex into lipid membranes will be enhanced and then blocking the Cu(II) binding sites in the enzymes of microorganisms.

3.6.2 | Antioxidant activities by DPPH radical scavenging activity

The free radical oxidative process plays a significant pathological role in causing many human diseases together with aging.[44] Thus, the antioxidant drugs are capable to protect the cells and organisms from damage caused by oxidative stress during metabolism. For this reason, there are extensive studies in literature to check the antioxidant activities of various synthetic compounds. There are many different methodologies used to study the antioxidant activities. The free radical DPPH˙ is commonly used for free radical scavenging determination due to its ease and convenience. In vitro antioxidant activity of the investigated complexes was evaluated by DPPH˙ free radical scavenging method. Antioxidant properties of the samples were measured using different concentrations (25, 50, 100, 150, and 200 μg/mL). For comparison, ascorbic acid was used as a standard. The % DPPH˙ scavenging values at 30-min incubation time are shown in Figure 8. It was observed that the antioxidant activities increased with increasing concentration of the complexes. It is worth to mention that at low concentration up to 100 μM, the percentage scavenging activities of the two complexes, **[Cu(L^1)$_2$]** and **[Co(L^3)$_2$]**, are higher than the standard. After that concentration (100 μM), all the scavenging activities of the complexes are smaller relative to the standard. In terms of IC_{50} (concentration of the sample required to inhibit 50% of radical), the data showed that **[Cu(L^1)$_2$]** complex has a potent antioxidant activity with the lowest IC_{50} value relative to other complexes (Figure 9). The IC_{50} order of the complexes is as follows: **[Cu(L^1)$_2$]** (52.3 μg/mL) < **[Co(L^3)$_2$]** (79.1 μg/mL) < **[Co(L^1)$_2$]** (101.3 μg/mL) < **[Ni(L^2)$_2$]** (107.5 μg/mL) < **[(NiL^3)$_2$]** (120.2 μg/mL) < **[Ni(L^1)$_2$]** (166.4 μg/mL).

TABLE 17 Antimicrobial activities of **HL^1** and its complexes

Compound	Inhibition zone diameter (mg/mm)	
	Escherichia coli (gram negative)	*Staphylococcus aureus* (gram positive)
HL^1	13	12
[Co(L^1)$_2$]	0.0	12
[Ni(L^1)$_2$]	11	10
[Cu(L^1)$_2$]	23	20
Ampicillin	25	21

3.6.3 | Fluorescence quenching studies

Fluorescence spectroscopy is an excellent and useful technique used to study the interactions between small molecules and macromolecules such as DNA.[45] This technique illustrates information about the binding properties (such as the binding mechanism, binding mode, binding constant, binding sites, and intermolecular distances) of the small molecules to protein/DNA.[46] Fluorescence quenching refers to any process that decreases the fluorescence intensity from a fluorophore induced by a variety of molecular interactions including

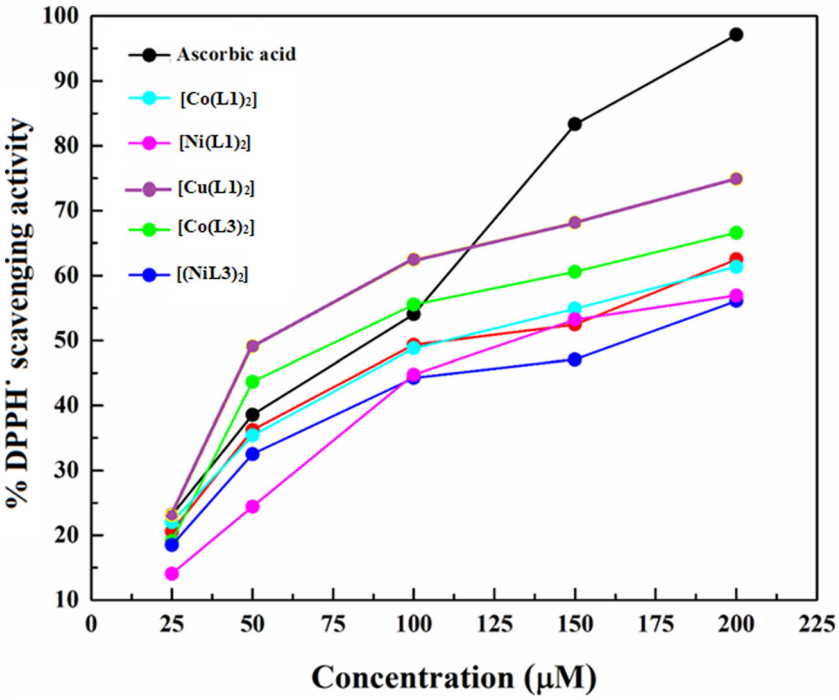

FIGURE 8 The percent DPPH˙ radical scavenging activities of the reported complexes compared with the standard ascorbic acid

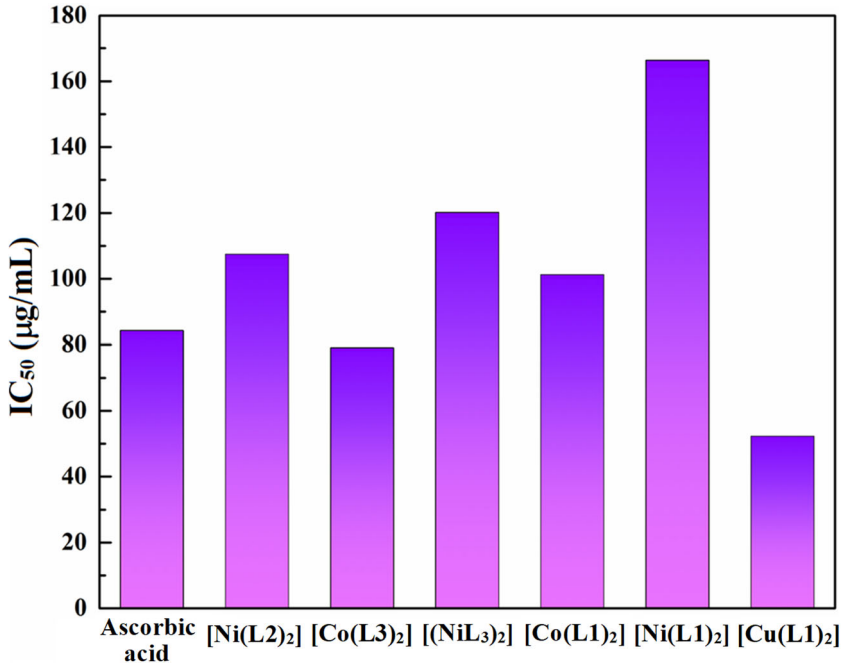

FIGURE 9 Trends in the inhibition of DPPH˙ radical by the investigated complexes

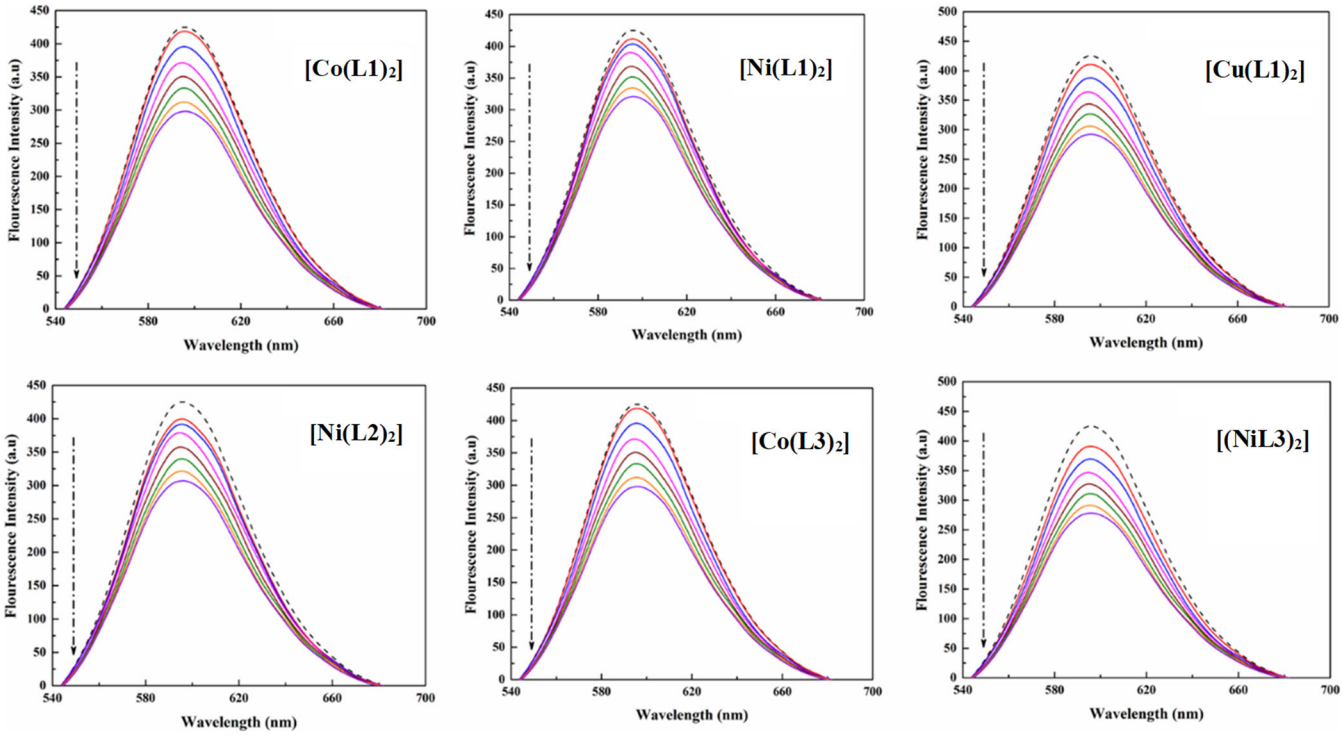

FIGURE 10 Fluorescence emission spectra of the EB–DNA system in the absence (dashed line) and presence (solid line) of reported complexes. Arrows indicate the intensity changes upon increasing the concentration of the complexes

excited-state reactions, molecular rearrangements, energy transfer, ground-state complex formation, and collisional quenching.[47] EB reagent is used to study the potential DNA-binding mode of the complexes. EB emits intense fluorescence band at 608 nm in the presence of CT-DNA due to the strong intercalation between it and the adjacent DNA base pairs. Addition of a second molecule that binds to DNA more strongly than EB will quench the DNA-induced EB emission.[44] Extent of quenching of the fluorescence of EB bound to DNA reflects the extent of the DNA binding to the added second molecule. The emission spectra of DNA bound to EB in the absence and presence of different concentrations of the investigated complexes are shown in Figure 10.

From figures, it can be noticed that addition of the complexes to CT-DNA pretreated with EB caused high reduction in emission intensity along with the increase in concentration of the reported derivatives. This indicates that the complexes strongly compete with EB and bind to DNA at the same sites occupied by EB. Fluorescence quenching occurs by dynamic and static quenching mechanisms. The dynamic mechanism results from collision between the quencher and the fluorophore, whereas the static mechanism can be due to the formation of a complex between the fluorophore and quencher.[48] The quenching constant, K_{sv}, is obtained from the slope of the linear plot $\{I_o/I$ versus $[Q]\}$. The plots (Figure 11) illustrate that the quenching of EB bound to CT-DNA by the complexes is in good agreement with the linear Stern–Volmer equation. The K_{SV} values were found to be **[Co(L^1)$_2$]** (0.93×10^4), **[Ni(L^1)$_2$]** (0.75×10^{-4}), **[Cu(L^1)$_2$]** (1.19×10^4), **[Ni(L^2)$_2$]** (0.78×10^4), **[Co(L^3)$_2$]** (0.97×10^4), and **[(NiL^3)$_2$]** (1.68×10^4), respectively.

3.6.4 | Viscosity measurements

Although the fluorescence quenching studies mentioned above offer essential information about the binding modes of complexes to DNA, they are lacking certain evidences to support an intercalative binding model.[49] Therefore, the interaction modes between the reported complexes and CT-DNA were further investigated by viscosity measurements to identify the effect of interaction on the length of CT-DNA (Figure 12). The hydrodynamic methods, which are sensitive to the change in DNA length, are regarded as the least obvious and most critical tests of binding in solutions. Intercalating agents increase the relative specific viscosity, $(\eta/\eta_o)^{1/3}$, of CT-DNA due to the elongation of the double helix to accommodate the compounds in between the base pairs. In contrast, a partial and/or nonclassical intercalation may bend or kink the DNA helix. Under the same conditions, typical results in less pronounced effect on its effective length and concomitantly its viscosity.[50] On increasing concentration of complexes, plots of relative viscosity versus [complex]/[DNA] exhibited significant increase in the viscosity of DNA solution. This indicates that complexes bind to CT-DNA through an intercalation binding mode.[51] The classical intercalators, such as EB, are known to increase the base pair separation, resulting in an increase in the relative viscosity of the CT-DNA. However, the effect of the transition metal complexes is less than that observed for EB intercalator, which indicated a weak intercalative interaction between the complexes and CT-DNA. The presence of transition metal complexes is accounting for the higher binding extent of the complexes with CT-DNA. The increased degree of viscosity, which may depend on its affinity to DNA, follows the order of **[Cu(L^1)$_2$]** > **[Ni(L^1)$_2$]** > **[Co(L^1)$_2$]** > **[Co(L^3)$_2$]**

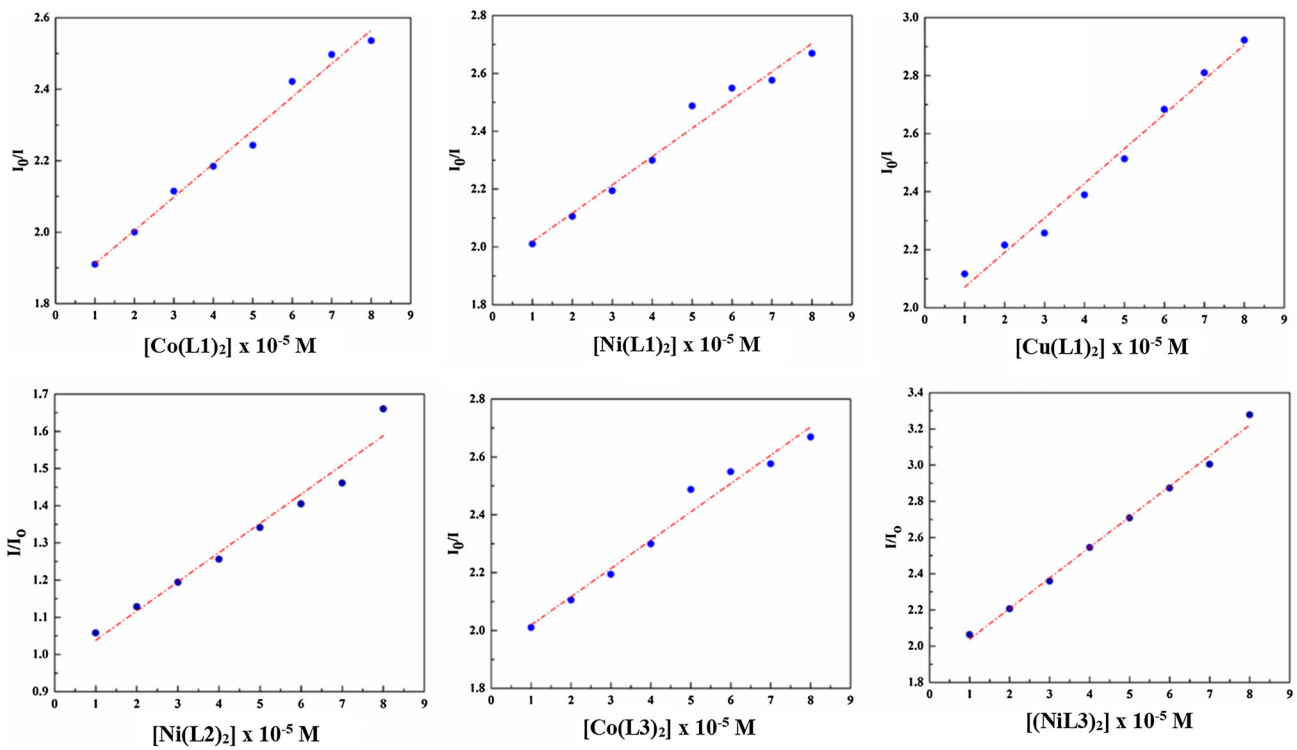

FIGURE 11 The profile of fluorescence variation of the studied complexes versus molar concentrations

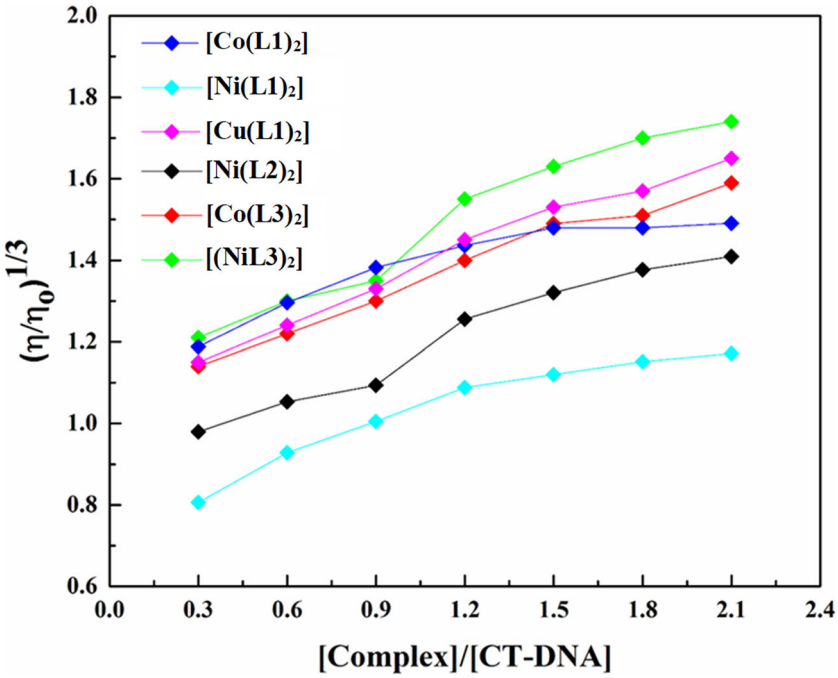

FIGURE 12 Effects of increasing the concentrations of the studied complexes on the relative viscosity of CT-DNA

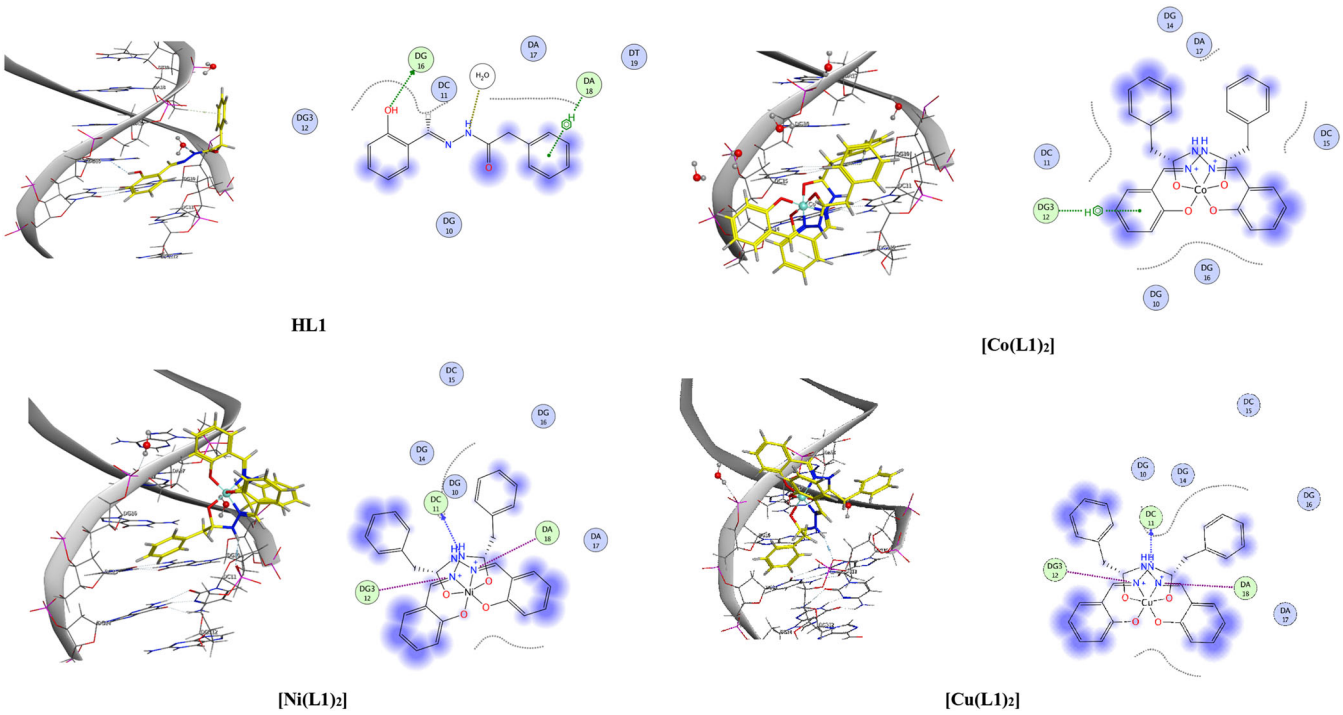

FIGURE 13 Molecular docking interactions (2D and 3D) of **HL**[1] and its complexes with DNA

> **[(NiL^3)$_2$]** > **[Ni(L^2)$_2$]**, which is consistent with the suggested hypothesis from fluorescence quenching data. The increased degree of viscosity showed that changing the metal environment could modulate the binding property of the complex with DNA.[52] Results of DNA binding studies confirmed the suggested intercalative mode mechanism for interaction between the compounds and DNA.

3.7 | Molecular docking studies

Molecular docking is a good theoretical process to declare the type of interaction between synthetic drugs and biological macromolecular target such as protein or DNA. The analysis is used to predict conformational changes associated with the amino acid moieties at the binding

position to accommodate the docked inhibitors. **HL^1** ligand and the reported complexes were subjected to molecular docking studies using the MOE version 2016.08 to identify the compound-DNA interactions (Figures 13 and 14). The docked ligand and complexes conformations were compared according to the binding energy, hydrophobic interactions, and hydrogen bonding between the compound and the B-DNA (PDB ID: 1BNA). The docking analysis determined the way by which the docked derivatives fundamentally fit with the DNA minor groove. It also demonstrated the hydrophobic, ionic, and hydrogen bonding interactions with the DNA base parts. It was found that most optimal docking fitted in the DG, DC, and DA regions. All the compounds displayed very good binding scores with high negative values (Table 18). This represents high binding affinity between the DNA receptor and indicates higher efficiency of the bioactive reagents. In the case of free **HL^1**, the binding interaction came from hydrogen bonds formed between DG16 and the OH group of ligand, as well as the interaction of DA18 with the phenyl moiety and hydrogen bonds formed between water molecules and the NH moiety of ligand (Figure 13). For **[Co(L^1)$_2$]** complex, the binding interaction came from hydrophobic interaction between amino acid moieties such as DA 17, DC 11, DC 15, and DG 16 with the aromatic moiety of the ligand as well as the interaction and hydrogen bonds of DG3 12 with the phenyl moiety. In the case of the three complexes, **[Ni(L^1)$_2$]**, **[Cu(L^1)$_2$]**, and **[Ni(L^2)$_2$]**, they showed similar interaction with the DNA (hydrogen bonding interactions with DA 18, DC 11, and DG3 12 regions as well as hydrophobic interactions with DA 17, DG 10, DC 15, and DG 16) (Figures 13 and 14). This could be due to their identical structures and similarity between the two ligands (Figure 2). The two complexes **[Co(L^3)$_2$]** and **[(NiL^3)$_2$]** interacted only through hydrophobic binding with DNA through the amino acid residues such as DG 10, DG 16, DA 17, DC 15, and DG3

TABLE 18 The values of final score functions of the interaction of DNA with **HL^1** and the reported complexes

Compound	S
HL^1	−5.1557
[Co(L^1)$_2$]	−5.4508
[Ni(L^1)$_2$]	−5.3070
[Cu(L^1)$_2$]	−5.2215
[Ni(L^2)$_2$]	−5.4531
[Co(L^3)$_2$]	−5.0700
[(NiL^3)$_2$]	−6.2719

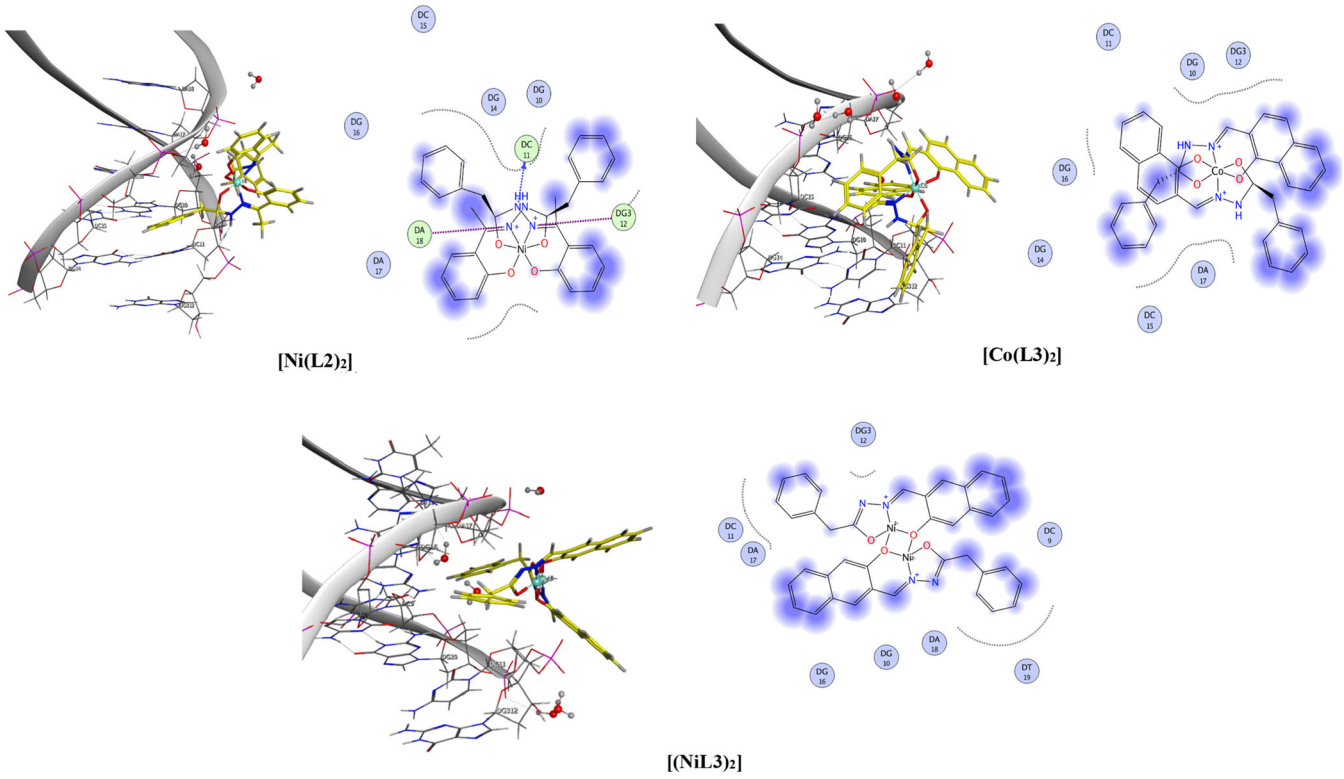

FIGURE 14 Molecular docking interactions (2D and 3D) of the complexes of **HL^2** and **HL^3** with DNA

12 and the aromatic moieties of the ligand (Figure 14). Interestingly, the dimer nickel(II) complex, **[(NiL^3)$_2$]**, exhibited the best binding score with a value of −6.2719 kcal mol^{-1}. This could be due to the presence of two metal species and the expanding structure, which gave more chance of binding (Figure 14). Therefore, it is obvious that these bioactive derivatives are effectively able to interact with the available binding sites of the macromolecule target. In addition, the theoretical studies supported the experimental findings of the fluorescence quenching and viscosity measurements, which indicated the intercalative mode for DNA interaction. The order of decreasing of binding interaction of the complexes is as follows: **[(NiL^3)$_2$]** > **[Ni(L^2)$_2$]** > **[Co(L^1)$_2$]** > **[Ni(L^1)$_2$]** > **[Cu(L^1)$_2$]** > **[Co(L^3)$_2$]**.

4 | CONCLUSION

Bivalent metal complexes with three hydrazide Schiff base derivatives revealed different structural features. The optimized molecular structures computed by DFT method were consistent with the experimental finding. Quantum and non-quantum global descriptors along with the NLO properties confirmed the effectiveness of the complexes as NLO candidates and showed that the complexation increased the NLO properties. Biological activities, fluorescence quenching, viscosity measurements, and molecular docking studies indicated that the reported complexes have good ability to bind with DNA. Therefore, they may be considered as promising potential drugs for therapeutic intervention for various diseases.

DATA AVAILABILITY STATEMENT

The data that support the findings of this study are available from the corresponding author upon reasonable request. Supporting information Files containing complete data for the crystal structures of **HL^1** have been submitted to the Cambridge Crystallographic Data Center with reference numbers CCDC deposition no. 1880657.

AUTHOR CONTRIBUTIONS

Ramadan Ramadan: Project administration; supervision. **Samir El-Medani:** Investigation; project administration; supervision. **Abdelmoneim Makhlouf:** Investigation; methodology; supervision. **Hussein Moustafa:** Data curation; formal analysis; software; validation. **Manal A. Afifi:** Data curation; formal analysis; investigation; methodology. **Matti Haukka:** Formal analysis; methodology; software; validation. **Ayman Abdel Aziz:** Data curation; formal analysis; methodology.

ORCID

Ramadan M. Ramadan https://orcid.org/0000-0002-9755-5410
Samir M. El-Medani https://orcid.org/0000-0002-7519-2241
Abdelmoneim Makhlouf https://orcid.org/0000-0001-7485-1834
Hussein Moustafa https://orcid.org/0000-0001-5707-4244
Manal A. Afifi https://orcid.org/0000-0002-5643-2991
Matti Haukka https://orcid.org/0000-0002-6744-7208
Ayman Abdel Aziz https://orcid.org/0000-0003-0041-6607

REFERENCES

[1] C. W. Dikio, B. J. Okoli, F. M. Mtunz, *Cogent Chemistry* **2017**, *3*, 1336864.
[2] S. M. El-Medani, A. A. Makhlouf, H. Moustafa, M. A. Afifi, M. Haukka, R. M. Ramadan, *J. Mol. Struct.* **2020**, *1208*, 127860.
[3] S. N. Battin, *Vanillin-Aminoquinoline Schiff Bases and Their Co (II), Ni (II) and Cu (II) Complexes*, Laxmi Book Publication, India **2019**.
[4] R. Gryboś, J. Szklarzewicz, A. Jurowska, M. Hodorowicz, *J. Mole. Struct.* **2018**, *1171*, 880.
[5] A. A. Abdel Aziz, F. M. Elantabli, H. Moustafa, S. M. El-Medani, *J. Mol. Struct.* **2017**, *1141*, 563.
[6] N. Vamsikrishna, M. P. Kumar, S. Tejaswi, A. Rambabu, *J. Fluoresc.* **2016**, *26*, 1317.
[7] S. Sathya Bama, S. Jayasurya, S. Sankaranarayanan, P. Bamas, *Int. J. Pharm. Sci.* **2012**, *4*, 557.
[8] M. Bal, G. Ceyhan, B. Avar, M. Kose, A. Kayraldiz, M. Kurtoğlu, *Turkish J. Chem.* **2014**, *38*, 222.
[9] E. Canpolat, H. Şahal, M. Kaya, S. Gur, *J. Chem. Soc. Pakistan* **2014**, *36*, 106.
[10] P. Subbaraj, A. Ramu, N. Raman, J. Dharmaraja, *Spectrochim. Acta, A* **2014**, *117*, 65.
[11] R. Kaplánek, M. Jakubek, J. Rak, Z. Kejík, M. Havlík, B. Dolenský, I. Frydrych, M. Hajdúch, M. Kolář, K. Bogdanová, J. Králová, P. Džubák, V. Král, *Bioorg. Chem.* **2015**, *60*, 19.
[12] M. Bingul, O. Tan, C. R. Gardner, S. K. Sutton, G. M. Arndt, G. M. Marshall, B. B. Cheung, N. Kumar, D. S. Black, *Molecules* **2016**, *21*, E916.
[13] B. Kocyigit-Kaymakcioglu, S. S. Yazici, F. Tok, M. Dikmen, S. Engür, E. E. Oruc-Emre, A. Iyidogan, *Lett. Drug des. Discovery* **2019**, *16*, 522.
[14] R. P. Bakale, G. N. Naik, C. V. Mangannavar, I. S. Muchchandi, I. N. Shcherbakov, C. Frampton, K. B. Gudasi, *Eur. J. Med. Chem.* **2014**, *73*, 38.
[15] H.-Q. Chang, L. Jia, J. Xu, W.-N. Wu, T.-F. Zhu, R.-H. Chen, T.-L. Ma, Y. Wang, Z.-Q. Xu, *Trans. Met. Chem.* **2015**, *40*, 485.
[16] C. Marzano, M. Pellei, F. Tisato, C. Santini, *Anti-Cancer Agents Med. Chem.* **2009**, *9*, 185.
[17] I. Iakovidis, I. Delimaris, S. M. Piperakis, *Molecular Biology International* **2011**, *2011*, 594529.
[18] A. F. H. Noureldeen, S. Y. Qusti, W. A. Alamoudi, A. I. Rawas, R. M. Ramadan, *Adv. Environm. Biologia* **2016**, *10*, 159.

[19] A. F. H. Noureldeen, H. M. Gashlan, S. Y. Qusti, R. M. Ramadan, *Int. J. Pharmaceut. Phytopharmacol. Res.* **2017**, *7*, 7.
[20] D. Gewirth, *An Oscillation Data Processing Suite for Macromol. Cryst*, 6th ed., Yale University, New Haven, Connecticut, USA **2003**.
[21] G. M. Sheldrick, *SADABS e Bruker AXS Scaling and Absorption Correction*, Bruker AXS, Inc., Madison, Wisconsin, USA **2012**.
[22] G. M. Sheldrick, *Acta Cryst.* **2008**, *A64*, 112.
[23] E. F. Pettersen, T. D. Goddard, C. C. Huang, G. S. Couch, D. M. Greenblatt, E. C. Meng, *J. Comput. Chem.* **2004**, *25*, 1605.
[24] L. J. Barbour, *J. Supramol. Chem.* **2001**, *1*, 189.
[25] Z. Otwinowski, W. Minor, Processing of X-ray diffraction data collected in oscillation mode, in *Macromolecular Crystallography, Part A*, (Eds: C. W. Carter Jr., R. M. Sweet, A. Press) Methods in Enzymology Vol. 276 **1997** 307.
[26] M. J. Frisch, H. B. Schlegel, G. E. Scuseria, M. A. Robb, J. R. Cheeseman, G. Scalmani, V. Barone, B. Mennucci, G. A. Petersson, H. Nakatsuji, M. Caricato, X. Li, H. P. Hratchian, A. F. Izmaylov, J. Bloino, G. Zheng, J. L. Sonnenberg, M. Hada, M. Ehara, K. Toyota, R. Fukuda, J. Hasegawa, M. Ishida, T. Nakajima, Y. Honda, O. Kitao, H. Nakai, T. Vreven, J. A. Montgomery Jr., J. E. Peralta, F. Ogliaro, M. Bearpark, J. J. Heyd, E. Brothers, K. N. Kudin, V. N. Staroverov, R. Kobayashi, J. rmand, K. Raghavachari, A. Rendell, J. C. Burant, S. S. Iyengar, J. Tomasi, M. Cossi, N. Rega, J. M. Millam, M. Klene, J. E. Knox, J. B. Cross, V. Bakken, C. Adamo, J. Jaramillo, R. Gomperts, R. E. Stratmann, O. Yazyev, A. J. Austin, R. Cammi, C. Pomelli, J. W. Ochterski, R. L. Martin, K. Morokuma, V. G. Zakrzewski, G. A. Voth, P. Salvador, J. J. Dannenberg, S. Dapprich, A. D. Daniels, O. Farkas, J. B. Foresman, J. V. Ortiz, J. Cioslowski, D. J. Fox, Gaussian Inc., Wallingford, CT, **2009**.
[27] R. G. Mohamed, A. A. Makhlouf, S. A. Mosad, A. A. Abdel Aziz, S. M. El-Medani, R. M. Ramadan, *J. Coord. Chem.* **2018**, *71*, 3665.
[28] Y. Ünver, K. Sancak, F. Çelik, E. Birinci, M. Küçük, S. Soylu, N. A. Burnaz, *Eur. J. Med. Chem.* **2014**, *84*, 639.
[29] T. F. Tullis, *Metal-DNA Chemistry*, ACS Symposium Series Vol. 402, American Chemical Society, Washington DC, USA **1989**.
[30] M. J. Waring, *J. Mol. Biol.* **1965**, *13*, 269.
[31] R. M. Ramadan, A. K. A. Al-Nasr, A. F. H. Noureldeen, *Spectrochim. Acta, A* **2014**, *132*, 417.
[32] R. M. Claramunt, C. Lopez, M. D. Santa Maria, D. Sanz, J. Elguero, *Prog. Nucl. Mag. Reson. Spec.* **2006**, *49*, 169.
[33] K. Nakamoto, *Infrared and Raman Spectra of Inorganic and Coordination Compounds, Part B*, 6th ed., John Wiley & Sons, Inc., Hoboken, New Jersey **2009**.
[34] A. Sankaraperumal, J. Karthikeyan, A. N. Shetty, R. Lakshmisundaram, *Polyhedron* **2013**, *50*, 264.
[35] E. A. El-Samanody, *Appl. Organometal. Chem.* **2018**, *32*, e4586.
[36] J. Wang, X.-Q. Xie, T. Hou, X. Xu, *J. Phys. Chem. A* **2007**, *111*, 4443.
[37] P. P. Kapupara, C. R. Matholiya, A. S. Dedakiya, T. R. Desai, *Int. Bull. Drug Res.* **2011**, *1*, 1.
[38] M. Andrasi, P. Buglyo, L. Zekany, A. Gaspar, *J. Pharm. Biomed. Anal.* **2007**, *44*, 1040.
[39] Y. Y. Lin, N. P. Rajesh, P. S. Raghavan, P. Ramasamy, Y. C. Huang, *Mater. Lett.* **2002**, *56*, 1074.
[40] L. Armelao, S. Quici, F. Brigelletti, G. Accorsi, G. Bottaroi, M. Cavazzini, E. Tendello, *Coord. Chem. Rev.* **2010**, *254*, 487.
[41] N. A. Smith, P. Zhang, S. E. Greenough, M. D. Horbury, G. J. Clarkson, D. McFeely, A. Habtemariam, L. Salassa, V. G. Stavros, C. G. Dowson, P. J. Sadler, *Chem. Sci.* **2017**, *8*, 395.
[42] D. W. Deamer, A. Kleinzeller, D. M. Fambrough (Eds), *Membrane Permeability: 100 Years since Ernest Overton, Current Topics in Membranes*, Vol. 48, Academic Press, San Diego, CA **1999**.
[43] B. G. Tweedy, *Phytopathology* **1964**, *55*, 910.
[44] Z.-C. Liu, B.-D. Wang, Z.-Y. Yang, Y. Li, D.-D. Qin, T.-R. Li, *Eur. J. Med. Chem.* **2009**, *44*, 4477.
[45] M. Sirajuddin, S. Ali, A. Badshah, *J. Photochem. Photobiol. B* **2013**, *124*, 1.
[46] J. Zhang, X. J. Wang, Y. J. Yan, W. S. Xiang, *J. Agric. Food Chem.* **2011**, *59*, 7506.
[47] P. Sathyadevi, P. Krishnamoorthy, M. Alagesan, K. Thanigaimani, P. Thomas Muthiah, N. Dharmaraj, *Polyhedron* **2012**, *31*, 294.
[48] F. Samari, B. Hemmateenejad, M. Shamsipur, M. Rashidi, H. Samouei, *Inorg. Chem.* **2012**, *51*, 3454.
[49] L. Jia, P. Jiang, J. Xu, Z. Y. Hao, X. M. Xu, L. H. Chen, J. C. Wu, N. Tang, Q. Wang, J. J. Vittal, *Inorg. Chim. Acta* **2010**, *363*, 855.
[50] S. Satyanarayana, J. C. Dabrowiak, J. Chaires, *Biochemistry* **1993**, *32*, 2573.
[51] S. Anbu, M. Kandaswamy, S. Kamalraj, J. Muthumarry, B. Varghese, *Dalton Trans.* **2011**, *40*, 7310.
[52] M. Kotoucek, J. Skopalova, D. Michalkova, *Anal. Chim. Acta* **1997**, *353*, 61.

SUPPORTING INFORMATION

Additional supporting information may be found online in the Supporting Information section at the end of this article.

How to cite this article: Ramadan RM, El-Medani SM, Makhlouf A, et al. Spectroscopic, density functional theory, nonlinear optical properties and in vitro biological studies of Co(II), Ni(II), and Cu(II) complexes of hydrazide Schiff base derivatives. *Appl Organomet Chem*. 2021; e6246. https://doi.org/10.1002/aoc.6246